

Review

# Atomic Force Spectroscopy on Ionic Liquids

Christian Rodenbücher \*, Klaus Wippermann and Carsten Korte

Forschungszentrum Jülich GmbH, Institute of Energy and Climate Research (IEK-3), 52425 Jülich, Germany; k.wippermann@fz-juelich.de (K.W.); c.korte@fz-juelich.de (C.K.)

\* Correspondence: c.rodenbuecher@fz-juelich.de

Received: 30 April 2019; Accepted: 24 May 2019; Published: 29 May 2019



**Abstract:** Ionic liquids have become of significant relevance in chemistry, as they can serve as environmentally-friendly solvents, electrolytes, and lubricants with bespoke properties. In particular for electrochemical applications, an understanding of the interface structure between the ionic liquid and an electrified interface is needed to model and optimize the reactions taking place on the solid surface. As with ionic liquids, the interplay between electrostatic forces and steric effects leads to an intrinsic heterogeneity, as the structure of the ionic liquid above an electrified interface cannot be described by the classical electrical double layer model. Instead, a layered solvation layer is present with a structure that depends on the material combination of the ionic liquid and substrate. In order to experimentally monitor this structure, atomic force spectroscopy (AFS) has become the method of choice. By measuring the force acting on a sharp microfabricated tip while approaching the surface in an ionic liquid, it has become possible to map the solvation layers with sub-nanometer resolution. In this review, we provide an overview of the AFS studies on ionic liquids published in recent years that illustrate how the interface is formed and how it can be modified by applying electrical potential or by adding impurities and solvents.

**Keywords:** ionic liquids; solid/liquid interface; atomic force microscopy; electric double layer

## 1. Introduction

In general, ionic liquids are defined as liquids that are composed entirely of ions [1]. This definition includes melts of crystalline ionic materials, which are commonly referred to as “molten salts”, as well as mixtures of any type of ions in the liquid state. In a narrower sense, “room-temperature ionic liquids (RTIL)” are understood as salts, which often contain organic ions, with melting points below room temperature [2,3]. Starting from their first discovery in 1914, they have become of central interest in fundamental and applied chemistry in recent decades, mainly because they are considered as promising alternative environmentally-beneficient solvents [4]. As their properties can be as systematically tailored as both their constituents, anion and cation, can be varied, they have been labelled “designer solvents” [5]. In general, ionic liquids provide a variety of desirable characteristics for chemical engineering, such as a high chemical and thermal stability, a high ionic conductivity, a negligible vapor pressure, and low flammability [6]. Potential fields of application comprise not only all techniques of chemical synthesis and processing where conventional molecular solvents are employed, but also mechanical engineering where ionic liquids may serve as lubricants and coatings [7]. Moreover, they have attracted enormous attention in electrochemistry, as they can be used as stable electrolytes for sustainable energy storage and conversion by supercapacitors, batteries, dye-sensitized solar cells, or polymer electrolyte membrane fuel cells (PEMFCs) [8]. As an illustration of the composition of ionic liquids, selected cations and anions are presented in Figure 1.

The analysis and description of ionic liquids opens a new field of science, not only because of the tremendous number of potential ionic liquids (up to  $10^6$  binary and  $10^{18}$  ternary ionic liquids

have been predicted [9]), but rather because ionic liquids behave fundamentally differently than conventional molecular solvents. Classically, liquids are understood as matter without inner structure and long-range ordering [10]. As experiments have shown that this does not hold true for ionic liquids, a paradigm shift in the understanding of their structure has occurred. As Hayes et al. [11] put it, molecular solvents can be described as “homogeneous, coherent, and essentially irregular”, but ionic liquids must be regarded as “nanoheterogeneous, coherent, and essentially regular”.

This regular ordering not only involves the bulk of ionic liquids but also surfaces and interfaces, which is of particular importance when using ionic liquids in electrochemical applications. In molecular solvents, the interface between a solid electrode and a liquid solvent can be described as the formation of a double-layer, as elaborated by Helmholtz, Gouy, Chapman, and Stern [12], but in ionic liquids, the internal ordering also influences the electrochemical processes at the interface [13]. Hence, a multitude of experimental approaches have been applied in order to elucidate the structure of ionic liquids at electrified interfaces. Among them, at first, electrochemical impedance spectroscopy (EIS) must be mentioned as a well-established method for estimating the average double layer thickness and the potential of zero charge (PZC) [14]. This method has been complemented by optical methods of interface analysis such as sum frequency generation vibrational spectroscopy (SFG), or infrared (IR) and Raman spectroscopy [15,16]. High-energy reflection and scattering using X-rays and neutrons have also been employed, revealing that ionic liquids form regular layers at the interface [17,18]. Direct mechanical access to the interface structure has been provided by using a surface force apparatus (SFA) to measure the thickness of anion and cation layers at the interface with utmost precision down to the Angstrom scale but averaging over a large contact area in the square micrometer range [19]. Hence, in recent years, atomic force microscopy (AFM) has become the method of choice for the direct investigation of ionic liquid interfaces, as it probes the layered structure locally by using a microfabricated tip with a radius of curvature of a few tens of nanometers [20]. Typically, force spectroscopy mode has been used, wherein the force between the tip operating in the liquid and the solid interface is recorded during approaching and retracting, which will thus be the focus of this review.

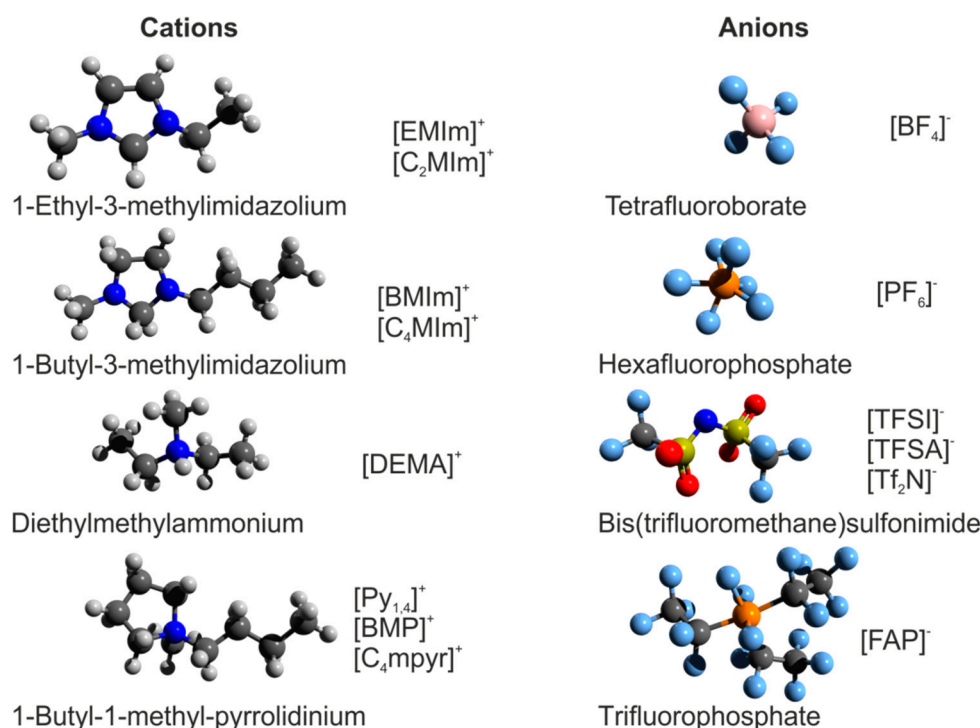


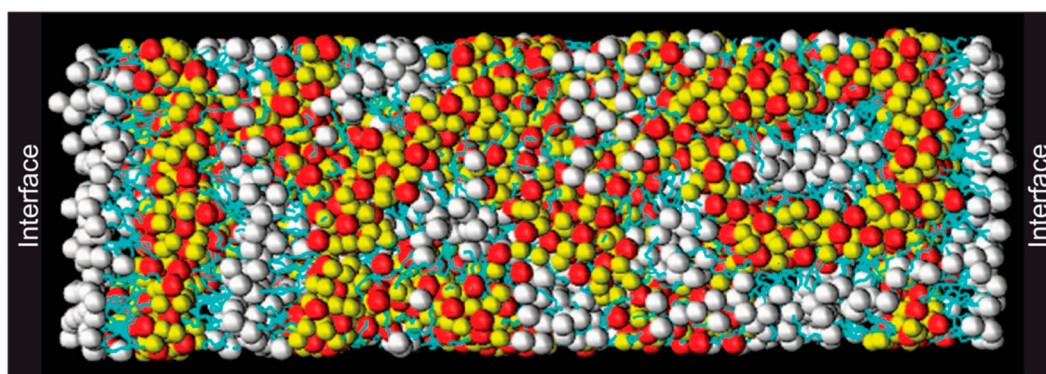
**Figure 1.** Ball-and-stick models of selected popular ionic liquid cations and anions. Note: A variety of abbreviations for the very same ions are used in the literature.

In the following, we will give a brief overview of the present knowledge on the bulk structure of ionic liquids and the formation of the interface layer to electrified surfaces before describing the measurement principle of atomic force spectroscopy. In the main part of this review, selected examples of AFM measurements in different modes are made, and the insights in the electrical double layer formed by ionic liquids and solid surfaces provided by this technique are discussed.

## 2. Bulk Structure of Ionic Liquids

As ionic liquids are composed of ions, the main interaction in the liquid phase is the electrostatic force between the oppositely-charged molecules. In contrast to a classical molten salt however, these molecules, in particular the cations, show a significant molecular asymmetry that countervails the coulombic interaction. This effect is the main cause of the characteristic low melting temperature [21,22]. Extensive theoretical and experimental research has been performed, especially on imidazolium-based ionic liquids, and it was found that they order in a self-assembled network, mediated by hydrogen bonding between the molecules in the solid as well as the liquid and even in the gas phase [23,24]. Hence, they can be effectively described as a heterogeneous polymeric “supramolecular fluid” consisting of polar and nonpolar domains at the nanoscale [25]. In order to illustrate the bulk structure of ionic liquids, simulations related to molecular dynamics, together with experimental high-energy scattering methods, are frequently employed [26].

When simulating the forces between the molecules, particular care must be taken into account for steric effects, since the electronic landscape around the ions in the liquid reveals a distinct anisotropy [27]. These effects can be exemplified with the imidazolium cations 1-ethyl-3-methylimidazolium [EMIm]<sup>+</sup> and 1-butyl-3-methylimidazolium [BMIm]<sup>+</sup> (see Figure 1). They both consist of a methyl group and an imidazole ring, while the length of their alkyl side chain differs. As the positive charge of the cation is located in the methyl head group, the tail group can be regarded as being nonpolar. By performing molecular dynamics simulations of ionic liquids consisting of imidazolium cations and NO<sub>3</sub><sup>-</sup> anions, Wang et al. [28] could show that the nonpolar tail groups of the cations mainly aggregate due to van-der-Waals forces. In this way, they form domains beside a network consisting of the head groups of the cations and anions, which is kept together by electrostatic forces. In this way, a heterogeneous nanostructure of the ionic liquid is established.



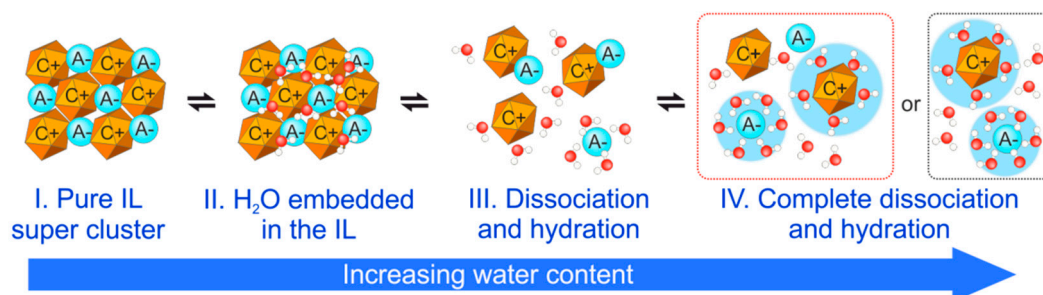
**Figure 2.** Molecular dynamics simulation of an ionic liquid consisting of imidazolium-based cations and NO<sub>3</sub><sup>-</sup> sandwiched between two vacuum interfaces. The white spheres represent the nonpolar cationic tail groups, the gold spheres the charged cationic head groups, the red spheres the anions, and the blue lines the cathodic side chains connecting the head and tail groups. Adapted from Wang et al. [28].

Figure 2 depicts a snapshot of such a simulation, making the aggregation phenomenon in the bulk visible. Comparing cations with different tail groups, Wang et al. [28] concluded that the tendency for building heterogeneous bulk structures increases with the length of the alkyl chains, which can explain many macroscopic properties such as diffusivity and viscosity. Not only does this hold true for the cations, but it was also found that asymmetric anions with extended alkyl chains can be the cause of

nanostructurization and domain formation. This opens up the opportunity to tailor ionic liquids with specific macroscopic properties by changing the configuration of their base ions [29,30]. Depending on the specific geometry of the ions, a variety of complex bulk structures can be adopted, e.g., for the protic ionic liquid ethylammonium nitrate ( $\text{EtNH}_3\text{NO}_3$ ), a defined structure composed of cationic layers with the anions distributed in between the layers as well as being intermixed with the cationic layers was proposed [31].

With the addition of further atomic species, the complexity increases. One example is triphilic ionic liquids, consisting of fluorinated, polar, and apolar constituents [32]. In these liquids, the cations typically contain the tails of alkyl chains while the anions have fluororous tails [33]. It was found that these fluororous tails agglomerate via self-assembly on the mesoscopic scale. Hence, three distinguishable types of domains are present, namely the charged polar domain, the fluorophilic domain and the lipophilic hydrocarbon domain [33]. They establish a filamentary network throughout the bulk phase of the liquid, thus introducing complex order phenomena [34]. As the building blocks of the network, which have fundamentally different local properties, coexist on the nanoscale, triphilic ionic liquids promise the possibility of the precise local control of chemical reactions and transport properties and thus have become an emerging research topic [33].

A further step towards more structural complexity is the admixture of additives or cosolvents, e.g., by mixing different ionic liquids [35]. When two or more ionic liquids are mixed, the resulting properties cannot be simply understood as conventional “double salt mixtures” but as all constituting ions interacting with each other, thus forming an individual nanostructure that determines the properties of the new liquid [36]. In pure ionic liquids, mixture effects related to impurities must also be considered. Water in particular is a common impurity, as it can be easily absorbed from a humid atmosphere or purposely added to the ionic liquid to alter the mechanical or electrochemical properties [37–40]. The uptake of water was found to depend specifically on the hydrophilicity of the anions, thus pointing to a close interaction between water and the ionic liquid nanostructure [41–43].



**Figure 3.** Schematic illustration of the mechanism of the intermixing between water and an ionic liquid. The ionic liquid is displayed in yellow (cations) and blue (anions) and the water in red (oxygen) and white (hydrogen). Adapted from Ma et al. [44].

In general, the addition of water to an ionic liquid can be divided into different steps, as elaborated by Ma et al. [44]. This scheme is illustrated in Figure 3. With small water contents, an embedding of water in the ionic liquid nanostructure can be established without clustering effects and thus this stage can be described as the solvent mixture (step II). With increasing water content, the ordered structure of the ionic liquid gets distorted and the dissociation and hydration occurs such that individual ion pairs can evolve (step III). Finally, at high water concentrations, a complete or partial dissociation and hydration takes place (step IV) and thus the mixture can be treated as a classical electrolyte. Depending on the individual properties of the ions, the solution of the ions in the water can also be related to the formation of micelles [45]. This has been studied in detail with ionic liquids containing the 1-alkyl-3-methylimidazolium family of cations and it has been found that the micelles formation can accelerate specific chemical reactions, thus showing potential for the practical application of ionic liquid-water mixtures in catalysis [46].

Considering the mechanisms of the formation of a heterogeneous nanostructure in the bulk of ionic liquids described so far, it must be expected that they will also influence the formation of the interface structure. As the presence of an interface breaks the symmetry of the system, a different nanostructure than that in the bulk evolves [47]. This can be readily seen in the simulation shown in Figure 2 where, at the surface of the liquid modelled as the interface to the vacuum, a preferential agglomeration of cationic tail groups occurs. When the ionic liquid is in contact with a solid, the interface structure is also affected by the topography, atomic arrangement, reactivity, local charge, and polarizability of the solid surface [11]. This interface structure becomes additionally distorted when electrical potential is applied to the solid, as is the case in electrochemical cells such as PEMFCs that employ ionic liquids as an electrolyte [48]. In consequence, a complex layered structure is formed in the ionic liquid that determines the kinetics of ion transport and reactions at the interface.

### 3. The Electric Double Layer at Solid-Liquid Interfaces

Investigations of the electric double layer formed in a liquid electrolyte close to an electrified interface range back to the early days of electrochemistry. In 1853, Helmholtz described the electric double layer as a simple capacitor formed by ions of the electrolyte being attracted by the oppositely-charged surface [49]. Later, Gouy and Chapman improved this conception by taking into account the fact that entropic effects lead to a smearing of the region that screens the surface charge and described the double layer as a diffuse space charge zone [50,51]. This model has been found to work well in describing electrolytes with low ion concentrations at moderate voltages. Stern further improved understanding of the interface by re-introducing a “Helmholtz-like” layer directly at the surface, thus removing the deficiencies that the Gouy–Chapman model revealed at high voltages, as it does not account for the finite size of the ions [52]. In this Gouy–Chapman–Stern model, a linear potential drop in the inner compact layer occurs before a quasi-exponential decrease in the outer layer does. An illustration of the discussed models of the electrical double layer is shown in Figure 4. These models are so-called “primitive models”, as they treat the ions as charged spheres, the solvent as a dielectric continuum, and the electrode as an ideal metal. When trying to understand the interface between an electrified solid surface and an ionic liquid, the above-mentioned models could not be successfully applied, mainly because they were developed for diluted electrolytes where the ion distribution can be described by Poisson–Boltzmann statistics [13]. To obtain a more comprehensive insight into the mechanism of the double layer, so-called “non-primitive models” were developed to take into account the properties of the metal electrode and the discrete nature of the solvent [53]. For instance, the ion-dipole-jellium model treats the solvent and solute as an ensemble of hard spheres interacting with the electron gas of the electrode [54,55]. In this way, it became possible to describe the processes at the interface with particular consideration of the charge transfer from a quantum mechanical perspective. However, for modelling ionic liquids, further parameters must be considered, as the electrolyte forms a kind of “ionic plasma” [56]. It was found that their electric double layer shows similarities to conventional molten salts, where overscreening or crowding effects become relevant [57]. Describing such a complex interface structure is challenging, and approaches using mean-field theory, Landau–Ginzburg theory, and molecular dynamics have been considered [13,57–59].

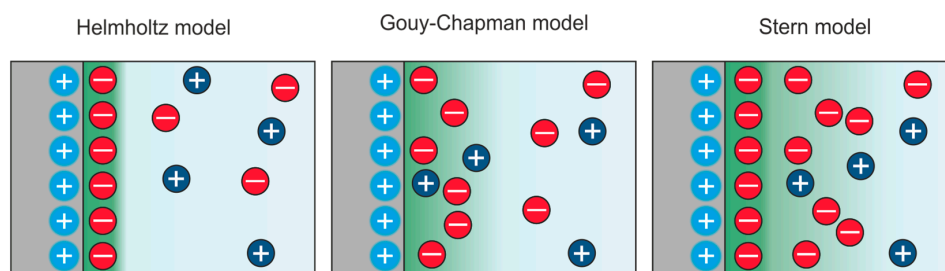


**Figure 4.** Models of the formation of the electrical double layer in an electrolyte in contact with a positively charged solid electrode.

As ionic liquids are entirely composed of ions, one can assume in a simplified approximation that ions with a charge opposite to the electrified electrode will be attracted to the interface. As illustrated in Figure 5 for a positive electrode, the first layer would be formed by anions, followed by a cation layer. Depending on the strength of the coulomb interaction, this layering will be repeated towards the bulk several times. With increasing distance from the interface, the disorder will decrease until, finally, the bulk structure is adopted. In ionic liquids composed of asymmetric ions, the orientation of the molecules also becomes relevant, and the interaction between charged head groups and uncharged tail groups can result in complex field-induced charge arrangement processes [60].

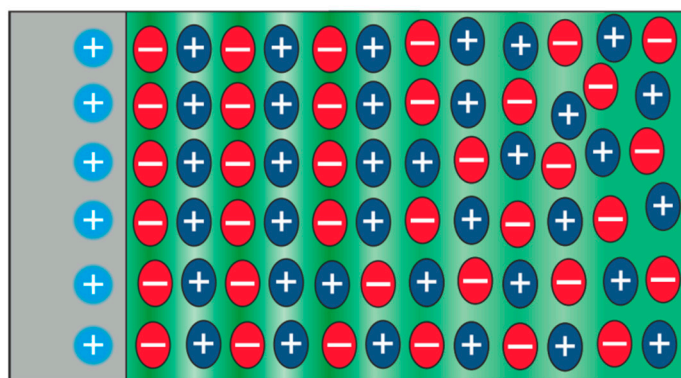


Figure 5. Simplified model of the interface between a positively-charged interface and an ionic liquid.

In order to verify or improve on these theories, direct experimental insight into the double layer structure is essential. In particular, the mechanical methods, AFM and SPA, have contributed significantly to elucidating the interface structure in recent years. While the AFM investigations will be discussed in detail below, we present as a first example SFA measurements performed on  $[C_4MIm][NTf_2]$  (also referred to as  $[BMIm][TFSI]$ ) by Gebbie et al. [61], illustratively revealing the shape of the extended double layer. As is shown in Figure 6, the force between a positive Au and a negative mica surface was measured to reveal an attraction starting at a distance of more than 25 nm before a repulsive force prevailed in the last nanometers in front of the surface. The data were modeled by the interplay of double layer attraction, van der Waals attraction, and steric repulsion. These results indicate that a long-range double layer, as well as a dense short-range nanostructure, which will be in the scope of the following discussion, exists simultaneously.

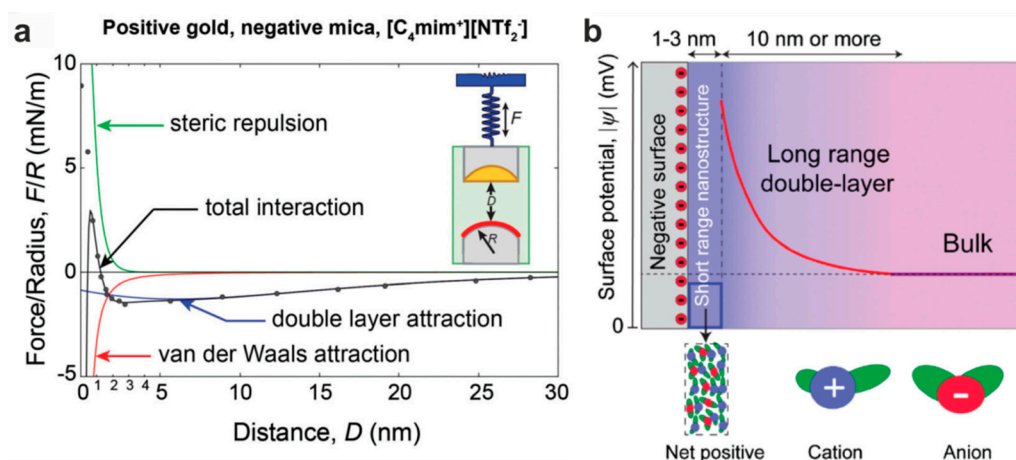


Figure 6. (a) SFA measurement of  $[C_4MIm][NTf_2]$  sandwiched between Au and mica; (b) resulting model of the electric double layer. Adapted from Gebbie et al. [61].

#### 4. Principles of Atomic Force Spectroscopy

Shortly after the epoch-making invention of the scanning tunneling microscope (STM), Binnig et al. developed the atomic force microscope (AFM) in the 1980s [62]. It utilizes a sharp tip attached to a microcantilever scanning the surface. In the standard contact mode, the deflection of the cantilever is measured via optical lever amplification when approaching the surface, thus serving as a force sensor based on Hooke's law:

$$F = -k\delta_c, \quad (1)$$

where  $F$  is the force,  $k$  the spring constant, and  $\delta_c$  the cantilever deflection [63]. Using a feedback loop, the force can be kept constant and thus the topography of solid samples can be mapped by moving the sample via piezo elements. With this relatively simple measurement technique, impressive results on the micro- and nanoscale, even up to atomic resolution, have been obtained [64]. As further measurement modes, the non-contact and intermittent or tapping mode have been developed based on the fact that the resonance frequency of the cantilever changes when the tip comes in the vicinity of a surface [65]. They are dynamic measurement modes, where the cantilever is oscillated and the frequency or amplitude of the oscillation is used as an input signal of the feedback loop. These techniques have the advantage that the direct interaction between the tip and sample is minimized, and thus more reliable measurements at higher scan speeds are possible. Dynamic measurements are not only possible using the optical lever technique but also with piezoelectric sensors such as the qPlus tuning fork, allowing for measurements with utmost signal-to-noise ratio [66,67].

AFM measurements can be performed in various environments without complex sample preparation and do not rely on the presence of vacuum conditions, which are required for other high-resolution microscopy techniques such as electron microscopy. Hence, the AFM has also become a versatile tool for the investigations of liquid samples in chemistry and life science [68]. It has been extensively employed for investigating the morphology changes of metallic surfaces during electrochemical polarization in various electrolytes, including ionic liquids [69–73].

Here, we focus on the investigation of the spatial extension of the electric double layer at a solid/liquid interface, where information about the structure out-of-plane, normal to the surface in particular, is needed. Therefore, the tip is approached and subsequently retracted from the surface and the force between the tip and sample is recorded as a function of their separation [74]. This mode is called atomic force spectroscopy (AFS), as the force-separation relationship depends on the material properties, thus allowing for mapping of the material contrast [63]. In recent years, AFS has become the method of choice for the investigation of interfaces in liquid and is in particular applied in nanobiology for investigating, e.g., cells, proteins, or antigen-antibody interactions [75]. During these investigations, where the samples are typically immersed in an ionic buffer, effects of interface modifications at charged surfaces have already become obvious [76].

Theoretically, the interaction between the tip and a solid surface can be approximated by the Lennard–Jones potential  $U_{LJ}$  (see Figure 7a), which was calculated by a two-atom approach. It includes an attractive van der Waals interaction and a repulsive interaction related to Coulomb forces and the Pauli Exclusion Principle:

$$U_{LJ} = -4\varepsilon \left( \frac{\sigma^6}{s^6} - \frac{\sigma^{12}}{s^{12}} \right) \quad (2)$$

Here,  $\varepsilon$  is the minimum of the potential well,  $s$  is the separation between the two atoms, and  $\sigma$  describes the separation of zero force [74]. On a real surface in contact with an ionic liquid, the situation can be more complex, as is illustrated by the schematic force curve shown in Figure 7b. At first, one must consider that in conventional AFMs, the force is recorded as a function of the position of the piezo scanner,  $z$ . This is, however, not the real distance between the tip and surface. As the cantilever is also moved by the piezo scanner when in contact with the surface, one must subtract the cantilever

deflection  $\delta_c$ , which has been measured by the optical lever method, from the scanner movement  $z$  in order to obtain the true distance, called separation  $s$ , between the tip and sample [77].

$$s = z - \delta_c \quad (3)$$

Secondly, one must consider that during approach and retraction, instabilities in cantilever motion can develop, leading to jumps [78]. When the gradient of the force between the tip and surface during the approach becomes larger than the spring constant of the cantilever, a jump-to-contact (JTC) occurs. Similarly, a jump-off-contact (JOC) occurs when the spring constant of the cantilever becomes larger than the gradient of adhesive forces between the tip and sample [79]. These two instabilities, related to the maximum adhesive forces called pull-on force and pull-off force, mark a hysteresis between the approach and the retraction curve, containing information about the material properties of the sample [78].

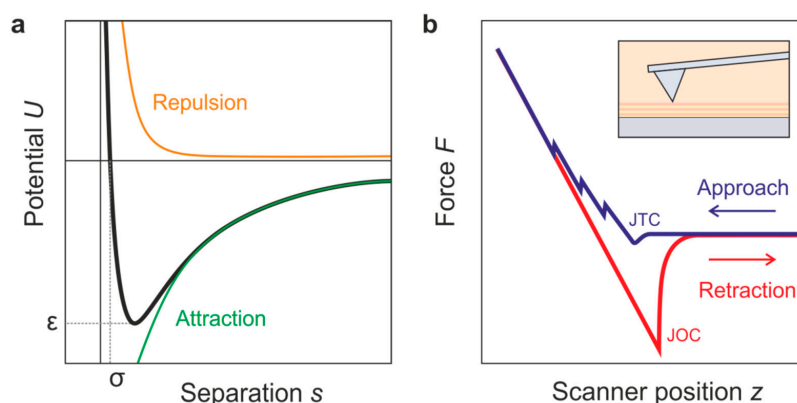


**Figure 7.** (a) Lennard–Jones potential describing the force between the tip and a solid surface related to attractive and repulsive interaction; (b) schematic illustration of a typical static-mode force curve obtained during approach and retraction of a solid surface in an ionic liquid.

When approaching solid surfaces in a liquid, the tip is not necessarily in direct contact with the surface after the jump-to-contact occurs, as solvation layers constitute an additional barrier that the tip must puncture before reaching the solid surface. Thanks to the high sensitivity of an AFM in the  $z$  direction, this effect can be used to resolve the internal structure of the interface layer. In the case of ionic liquids, dense alternating anion and cation layers are present at the interface that cause additional characteristic jumps in the force curve, preferentially during the approach, as illustrated in Figure 7b [80]. At each layer, the force increases at constant separation until it is high enough that the tip can puncture the layer and jump to the next layer. These jumps are strongly dependent on the charging of the system. In the case that the tip or surface is not charged, the measured thicknesses of the layers correspond to the dimension of the anion or cation, respectively, but when a charged surface is investigated with a charged tip, the observed jumps correlate with the dimension of an ion pair [81]. In this manner, detailed information about mechanical properties and the thicknesses of the interface layers of ionic liquids can be collected with sub-nN and sub-nm resolution.

In order to achieve such a high resolution, the condition of the tip is the key parameter. While extremely sharp Si tips can be prepared via microfabrication, their morphology is significantly altered by impurities. When handling the tips in ambient conditions, organic adsorbates can be adsorbed on the tip, impairing its performance. Hence, tip preparation methods involving plasma treatment, sputtering, or UV irradiation have been found to significantly increase the quality of AFM measurements in liquids [82]. A further source of tip contamination can be solid state impurities such as elements from the backside coating of the cantilever that have diffused to the tip apex [83]. Similar contaminations can also evolve in the course of the measurement if material from the solid surface or particles already present in the liquid get attracted to the tip and thus changing its geometry [84]. Besides these

unwanted effects, controlled tip modification by adsorbates can also be used to increase the sensitivity and selectivity of the tip as shown below [85].

A further parameter that can influence the measured forces is the velocity of the tip during approach and retraction. This has become obvious in particular when performing measurements in liquid for biological applications such as protein unfolding where the measured forces are related to the retraction speed [86,87]. Depending on the molecular structure of the interface, such dynamic processes also cannot be excluded when investigating ionic liquids by AFS and thus should be kept in mind.

## 5. Structure of the Interface Layer of Ionic Liquids Revealed by AFS

### 5.1. The Electrified Interface

The history of investigating the ionic liquid/solid interface layer by means of AFS goes back to the year 2006 when Atkin and Warr performed the first measurements on the atomically flat model substrates mica, silica, and graphite [88]. They investigated the three different ionic liquids 1-ethyl-3-methylimidazolium acetate ( $C_2MimAc$ ), propylammonium nitrate (PAN), and ethylammonium nitrate (EAN). As is exemplarily shown in Figure 8, the force–separation curves exhibit oscillations with frequencies corresponding to the dimension of the ion pairs of the respective ionic liquids. A strong correlation between the surface charge, surface roughness, and molecular arrangement with the observed layered structure was found. In particular, in the case of graphene, a pronounced layering was identified with up to seven layers for  $C_2MimAc$ . Hence, it was concluded that steric effects such as the local interaction of the alkyl chains of the ionic liquid molecules with the carbon atoms of the substrate are decisive for the formation of the interfacial structure. Comparing the ionic liquids under investigation, it has been determined that an increased internal flexibility (e.g., PAN compared to EAN) results in a weakening of the layer structure and an increase in the compressibility.

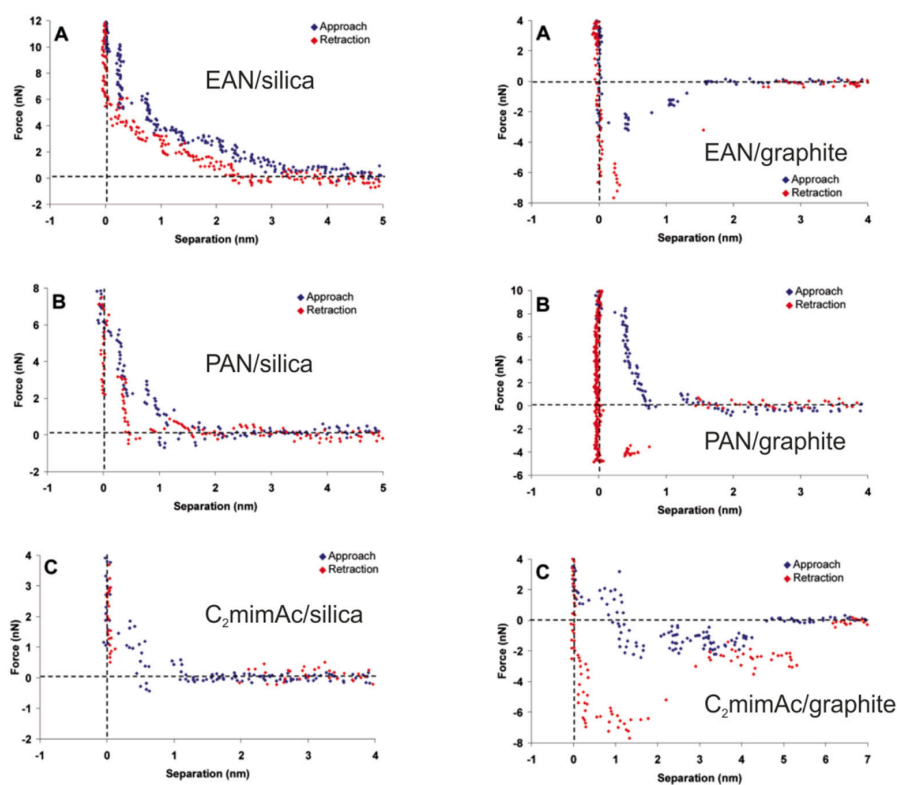


**Figure 8.** Force–separation curves measured on the silica surface (left) and the graphite surface (right) using three different ionic liquids, EAN (A), PAN (B) and  $C_2MimAc$  (C). Adapted with permission from Atkin and Warr [88]. Copyright 2007, American Chemical Society.

As the mechanical measurement of layered interfaces is prone to fluctuations, it is useful to not measure only one but a set of several tens of force curves (as drawback information about dynamic effects, which are often investigated in biological AFS, gets lost). Subsequently, their average can be calculated and presented using 2D histograms, as is shown for the [EMIm][TFSI]/mica interface in Figure 9. Four series of measurements obtained using different set points of maximum force are presented, illustrating a major challenge when performing AFS in liquids. Due to the calculation of the separation via the cantilever deflection (Equation (3)) and the increasing hardness of layers when approaching the surface, it is demanding to determine the point of zero separation, which denotes the point when the tip is in direct contact with the surface [20]. In all measurements, the layered interface structure of the ionic liquid can be clearly observed, but when choosing too low of a set point, the real surface cannot be reached. This also constitutes a requirement on the cantilever selection. Using a soft cantilever with a low spring constant has the advantage of high sensitivity at the expense of a limit on the maximum force. Furthermore, the large deflection of soft cantilevers can result in a distortion of the force curves due to the nonlinearities of the photodetector [20]. Hence, one should select a cantilever that can provide sufficient force to reach the surface. In the example of Figure 9, a set point of 14 nN was needed to puncture all liquid interface layers. This was concluded by the fact that a further increase of the force set point to 18 nN did not reveal further layers. An additional indication for hitting the surface can be derived by regarding the retraction curves, often showing a distinct change in adhesion after direct tip-surface contact [20].

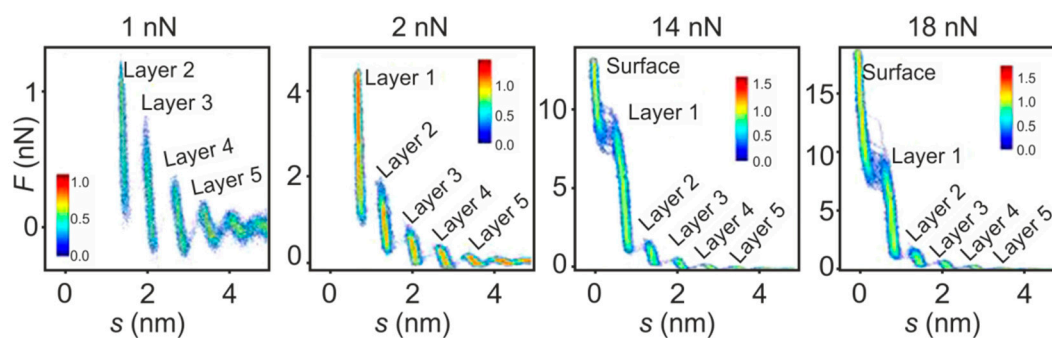


**Figure 9.** Force–separation curves measured during approach of the [EMIm][TFSI]/mica interface using different force set points. The 2D histograms were calculated using 50 curves. Adapted from Black et al. [20].

Using a tip attached to a cantilever as a mechanical probe, one should also keep in mind that the probe itself can have an impact on the measurement. The radius of commercial AFM tips is typically in the range of a few nanometers, which is much larger than the distance between ionic liquid interface layers that are supposed to be measured. Additionally, the presence of the tip leads to the formation of a second solid-liquid interface where, depending on the material and charge of the tip, a layered interface structure can also evolve. Hence, one interface structure is probed with another. Black et al. [20] performed tests employing two different tips on the same [EMIm][TFSI]/mica interface. They compared a SiN tip with a Au-coated SiN tip. As is shown in Figure 10, the layered interface structure can be seen in both measurements. The forces needed to puncture the layers are significantly different and mainly relate to the tip radius, which was up to three times higher for the Au-coated tip than for the uncoated one. Despite this, the measured thicknesses of the layers are the same for both tips, as becomes obvious from the separation histogram on the right of Figure 10.

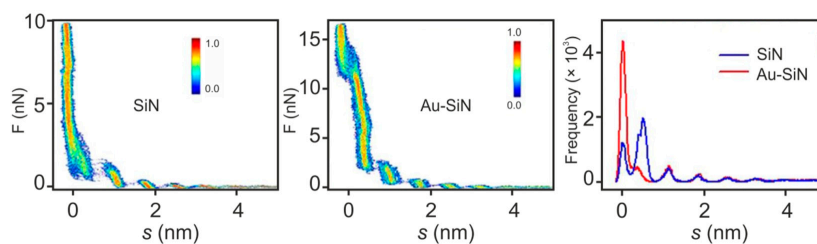


**Figure 10.** Force–separation curves and separation histogram measured during approach of the [EMIm][TFSI]/mica interface using comparing a SiN and a Au-coated SiN tip. Adapted from Black et al. [20].

In order to gain information on the electric double layer as a function of the electrical polarization of the solid surface, miniaturized electrochemical cells have been constructed and introduced in AFM setups. Hayes et al. [89] investigated the Au(111) surface in contact with the ionic liquids 1-ethyl-3-methylimidazolium tris(pentafluoroethyl) trifluorophosphate ([EMIm][FAP]) and 1-butyl-1-methylpyrrolidinium tris(pentafluoroethyl) trifluorophosphate ([Py<sub>1,4</sub>][FAP]) under different electrical polarizations. Figure 11 shows the resulting force–separation curves for the [Py<sub>1,4</sub>][FAP]/Au(111) interface at open circuit potential (OCP) and positive and negative voltage. The oscillatory behavior, which was already present at OCP, became modified upon polarization, leading to an increase in the force necessary to punctuate the innermost layers and an increase in the number of detected layers (Hoth et al. [90] even measured up to 12 ion pair layers at  $-2$  V). It has been observed that this effect is more pronounced at negative potentials, suggesting that the [Py<sub>1,4</sub>]<sup>+</sup> cations adsorbed on the surface are a more effective template for establishing an ordered interface structure.

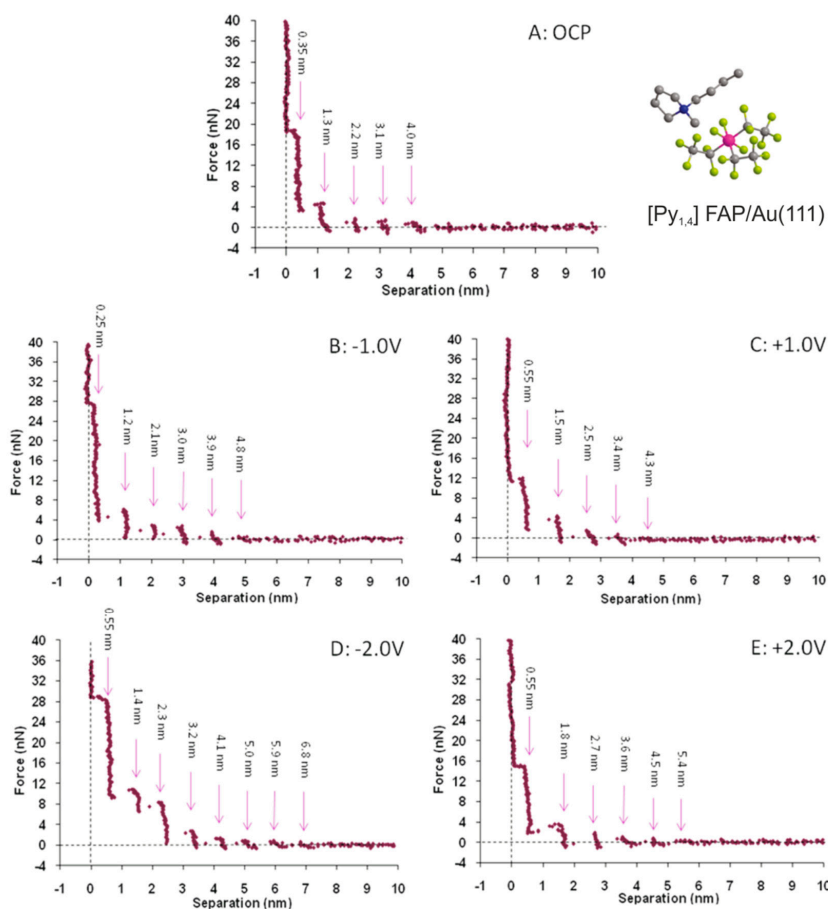


**Figure 11.** Force–distance measurements on the [Py<sub>1,4</sub>][FAP]/Au(111) interface at different surface potentials. Adapted with permission from Hayes et al. [89]. Copyright 2011, American Chemical Society.

These findings by Hayes et al. [89] finally provided direct experimental evidence that the electric double layer in ionic liquids cannot be traditionally described using a Gouy–Chapman–Stern approach, and an oscillatory capacitive double layer is present, as is illustrated in Figure 5. Hence, in recent years, AFS investigations under applied potential have been extended to a variety of different combinations of ionic liquids and conducting surfaces relevant for electrochemical applications [91,92]. For example, Zhang et al. [93] performed detailed measurements on the Au(111) surface in contact with 1-*n*-butyl-3-methylimidazolium hexafluorophosphate ([BMIm][PF<sub>6</sub>]). They were able to resolve three to four layers using AFS at the interface. By recording force–separation curves at potentials between −0.9 V and +0.5 V, they concluded that the electric double layer is confined to a few charged interior layers, but that additionally neutral exterior layers are also present.

The complexity of the interface structure under electrical polarization has been further elucidated by combining AFS investigations with STM mapping. For both investigated ionic liquids [Py<sub>1,4</sub>][FAP] and [EMIm][FAP], the innermost ions interact strongly with the electrode surface depending on the potential [94]. However, significant differences between the two liquids are present, considering surface reconstruction. While the [Py<sub>1,4</sub>][FAP]/Au interface undergoes herringbone reconstruction in the cathodic regime [95], no reconstruction has been observed for [EMIm][FAP]/Au [94]. Similar effects have been observed comparing 1-ethyl-3-methylimidazolium bis[(trifluoromethyl)-sulfonyl]amide ([EMIm][TfSA]) and 1-butyl-1-methylpyrrolidinium bis[(trifluoromethyl)-sulfonyl]amide ([Py<sub>1,4</sub>][TfSA]). Unlike the [EMIm]<sup>+</sup> cations, the [Py<sub>1,4</sub>]<sup>+</sup> cations were found to be strongly bound to the surface, leading to the evolution of a wormlike reconstruction pattern under cathodic polarization [96]. This illustrates that even small changes in the molecular configuration of the cations can drastically change the electrochemical properties of the ionic liquid. Moreover, the configuration of the anions can also have an impact on the interfacial structure as was addressed, e.g., by Liu et al. [97]. In their work, ionic liquids having the same [EMIm]<sup>+</sup> cation but four different anions bis(trifluoromethylsulfonyl)imide [TfSI]<sup>−</sup>, trifluoromethylsulfonate [TfO]<sup>−</sup>, methylsulfonate [Oms]<sup>−</sup>, and acetate [OAc]<sup>−</sup> were investigated in contact with the Au (111) surface. AFS measurements under cathodic polarization revealed that the number of layers and force necessary for their punctuation increases systematically with anion size, and it was concluded that this is also the cause for differences in macroscopic electrowetting behavior [97].

In order to extract further information from the force–separation curves, approaches to controlled tip modification have been developed. One method to enlarge and accurately define the size of the contact area is to use colloidal probes instead of conventional pyramidal AFM tips [98]. Using a spherical silica probe with a diameter of 5 μm, Li et al. [99] were able to elucidate the interface structure between Au and imidazolium-based ionic liquids with cations having different alkyl chain lengths, such as [EMIm]<sup>+</sup>, [BMIm]<sup>+</sup>, and [HMIm]<sup>+</sup>. They found that under cathodic polarization, [BMIm]<sup>+</sup> was relatively weakly bound to the surface, while [EMIm]<sup>+</sup> as well as [HMIm]<sup>+</sup> showed stronger interactions. For [EMIm]<sup>+</sup>, this was attributed to the stronger interaction of the imidazolium ring with the surface. For [HMIm]<sup>+</sup>, steric effects related to the increased length of the alkyl chain, leading to a stronger solvophobic force, have been made responsible. A second approach of tip modification was followed by Zhong et al. [85]. They attached alkylthiols with different end groups, such as −NH<sub>3</sub><sup>+</sup>, −COO<sup>−</sup>, and −CH<sub>3</sub> to the tip, thus creating charge-sensitive probes, as illustrated in Figure 12a. They investigated the interface between 1-octyl-3-methylimidazolium hexafluorophosphate ([OMIm][PF<sub>6</sub>]) and Au (111). Regarding the force–distance curves in Figure 12a measured under anodic and cathodic substrate polarization, distinct differences between the neutral, positive, and negative tips can be seen. Positively charged tips are more sensitive for layer detection at positive substrate potential and vice versa. This becomes obvious with regard to the force, which is necessary to punctuate the third sublayer as a function of the potential (Figure 12b). A “camel-shaped” dependency can be observed for all tips, indicating that the structural organization of the electric double layer increases with the potential at both polarities, but at positive potential, the positively-modified tips show the highest force, while at negative potential, the force for the negatively modified tips is the highest. Based on these findings, Zhong et al. [85] elaborated a molecular model of the interface, as shown in Figure 12c.

At negative substrate potential, the cations are modeled to be directly attached to the surface via their imidazolium ring where the positive charge is located. At positive bias, the smaller anions form the first interface layer with the cationic imidazolium ring attached to it while the cationic tail groups are pointed away from the surface. In the intermediate state, at zero charge, a checkerboard-like arrangement of the ions was assumed instead.

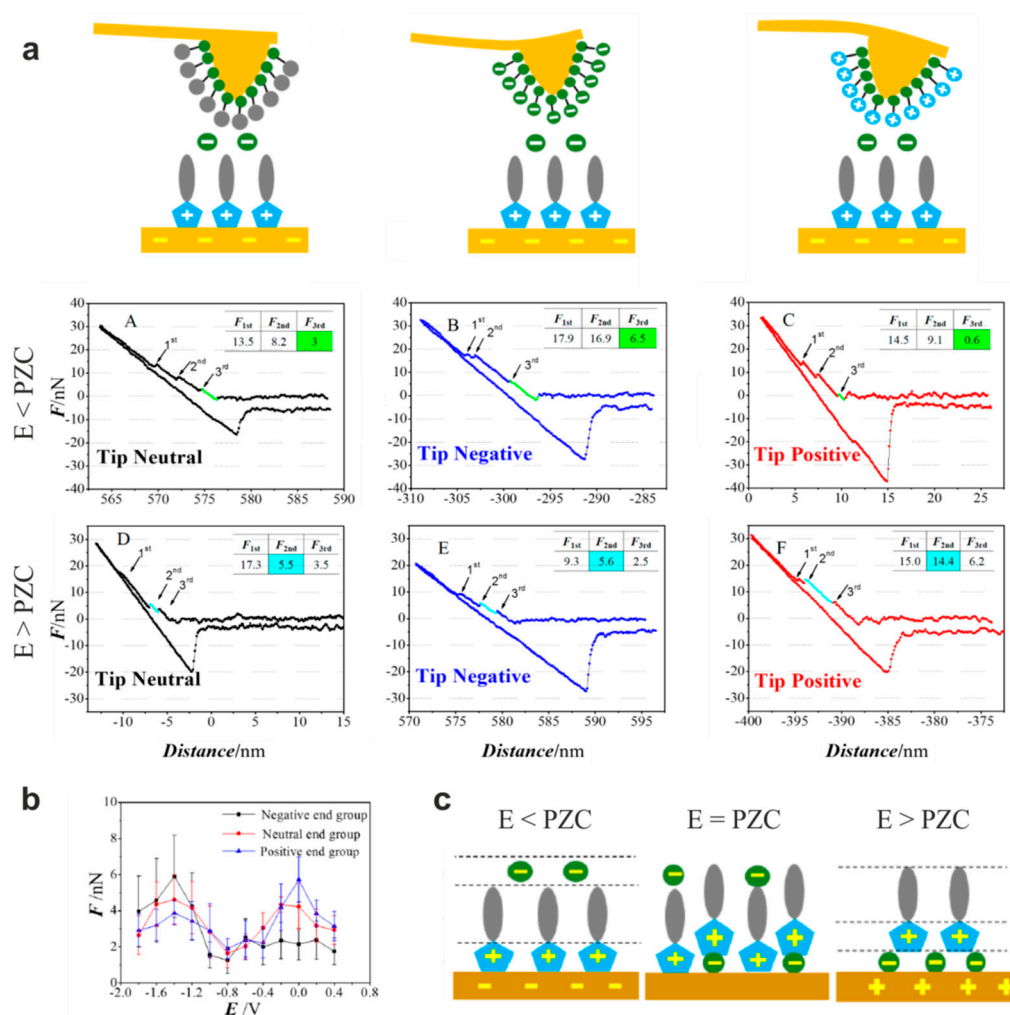


**Figure 12.** Measurement of the [OMIm][PF<sub>6</sub>]/Au(111) interface using a modified tip. (a) Force–distance curves measured at a potential (E) above and below the potential of zero charge (PZC) with molecules having neutral, negative, and positive end groups attached to the tip (the inset tables display the force necessary to rupture the first, second, and third layer); (b) force necessary to rupture the third sublayer measured at different potentials applied to the surface; (c) model of arrangement of the ionic liquid at the interface depending on the potential. Adapted from Zhong et al. [85].

Aside from the aforementioned investigations of the electrified Au surface, studies of the interface between ionic liquids and graphite have been conducted, as the understanding of carbon-based electrodes is of high significance for building fuel cells or electrochemical supercapacitors [100]. Black et al. [101] focused on the interface structure between 1-ethyl-3-methyl-imidazolium bis(trifluoromethanesulfonyl)imide ([EMIm][TFSI]) and highly oriented pyrolytic graphite (HOPG). The measured 2D force–separation histograms are presented in Figure 13 for the unbiased and positively and negatively polarized surface. In all cases, an ordered structure with up to four layers has been revealed. In order to gain a deeper insight into the ionic arrangement of the double layer, the measured curves were correlated with molecular dynamics simulations. The densities of anions and cations as a function of the separation from the surface were calculated from simulations performed at different

surface potentials, as shown in Figure 13 for +1 V and −1 V. In contrast to the uncharged surface, where different ion orientations are present, the electrostatic force induced by the application of the potential leads to a predetermined ion orientation in the first ion layer and a charge screening confined to approximately 1 nm. Further from the surface, a layered interface structure with absent preferential ion orientation was predicted. The conclusions derived from the simulation closely match the experimental results, showing the versatility of AFS for investigating the electric double layer in ionic liquids. Jurado et al. [102] extended the investigations of carbon-based materials to the graphene surface. They investigated the interface formed with [EMIm][TFSI] at zero charge as well as under applied potential, concluding that the strong interaction of the imidazolium ring with the graphene surface via  $\pi$ - $\pi$  bonding results in a preferential orientation of the ions and to an overscreening, even on the uncharged surface. When a potential was applied, the behavior of the double layer changed from overscreening towards crowding, leading to a decrease in the force within the layered structure.

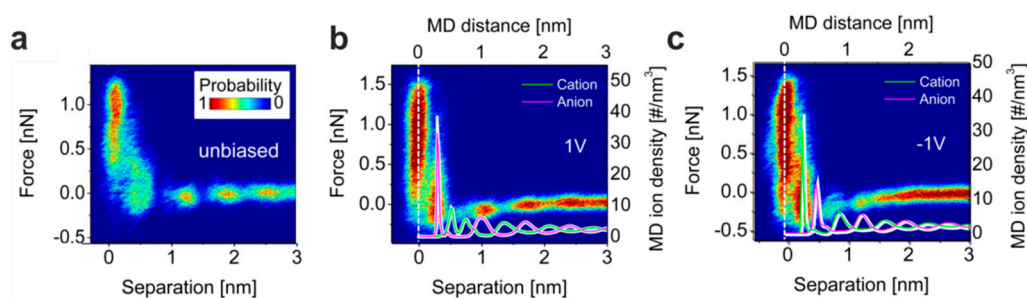


**Figure 13.** Atomic force spectroscopy (AFS) measurement of the [EMIm][TFSI]/HOPG interface (a) with unbiased surface, (b) at +1V, and (c) at −1V sample polarization; (b,c) additionally show the ion density of anions and cations derived by molecular dynamics at the interface, depending on the potential. Adapted with permission from Black et al. [101]. Copyright 2013, the American Chemical Society.

While the investigation of model systems of atomically flat surfaces provides valuable insights into the fundamental nature of the double layer formation of ionic liquids, one must question if these results can be directly transferred to real applications where rough electrodes are present. In order to scrutinize this issue, Sheehan et al. [103] conducted a study employing silica nanoparticles deposited on silica wafers. Additionally, they employed sharp tips as well as different silica colloids as AFM probes to modulate the roughness of the system confining the ionic liquid. Comparing the force curves measured in [HMIm][TFSI] shows that the roughness has a distinct influence on the layered structure. The presence of only a low density of nanoparticles modifies the measured double layer across the entire surface. Furthermore, the use of a rough probe contact was found to be related to a localized arrangement and agglomeration of the ionic liquid at “multi-asperity” contacts [103]. These results show that the presence of rough surfaces introduces further complexity to the system, affecting the static structure of the ionic liquids as well as their dynamics.

It should also be noted that although an ordered double layer structure at solid/liquid interfaces has been observed by AFS as well as by complementary methods on a large variety of ionic liquids, there seems to be no universal behavior. As a counterexample, Radiom et al. [104] reported on the interface between trihexyl(tetradecyl)phosphonium bis(mandelato)borate ([P<sub>6,6,6,14</sub>][BMB]) and different atomically flat surfaces, such as Au, mica, or silica. By investigating force–separation curves, no hints of the presence of a multilayer structure, but only a diffuse repulsion, were found. A possible explanation for this striking difference to conventional ionic liquids was suggested with regard to the molecular structure of [P<sub>6,6,6,14</sub>][BMB] having a large and flexible anion with delocalized charge and a compact and inflexible cation [104]. This combination could exclude a regular arrangement of the molecules at the interface. Furthermore, Cheng et al. [105] reported that even on popular imidazolium-based ionic liquids such as [EMIm][TFSI], no structured interface to mica is present if no water is present, as is discussed in detail below. This shows that the properties of ionic liquid/solid

interfaces are individual and must be investigated for every class of liquids, as well as for the specific boundary conditions, separately.

### 5.2. Influence of Water

When hydrophilic ionic liquids are employed for applications under environmental conditions, water is the major impurity that significantly influences the nanoscale structure of the double layer [106,107]. In particular, in ionic liquids used as electrolytes in fuel cells, water is generated as the product of the reaction between hydrogen and oxygen and can thus alter the reactions at the electrode surfaces [41]. Even small amounts of water can modify the interface structure of an ionic liquid under applied electric potential [108]. On the interface between butyl-1-methylpyrrolidinium bis(trifluoromethylsulfonyl) amide ([BMP][TFSA], also referred to as [Py<sub>1,4</sub>][TFSI]) and Au(111), Zhong et al. [109], using AFS, observed that upon a water increase from 30 ppm to 90 ppm, the stiffness of the first interface layers decreased significantly while the thickness of the layers increased. This indicates that at this low concentration, water absorbs on the surface and distorts the defined orientation of ions in the layer. A comparable result was obtained by Wang et al. [110] on different 1-alkyl-3-methylimidazolium bis(trifluoromethanesulfonyl) imide ([C<sub>n</sub>Mim][TFSI]) ionic liquids. Water was found to distort the interfacial structure formed with mica, which also impacts the wetting behavior of the liquid [111]. The dissolution of the structured interface layer upon water uptake is also a challenge when using ionic liquids as lubricants due to higher friction [112].

In contrast to many reports showing that even small amounts of water lead to a distortion of the structured interface layer, Cheng et al. [105] note that the presence of water is necessary for the evolution of a layered structure at the interface. They also investigated [RMIm][TFSI] ionic liquids in contact with mica and found that the force-separation curves were not indicative for a layered interface structure when using carefully dried ionic liquids, as is shown in Figure 14a,b. The force curve was found to be continuous with a repulsive force detected from approximately 12 Å away from the surface, which reveals that only an unstructured interface layer exists. Only after exposing the ionic liquid to humid ambient conditions could the characteristic instabilities in the force curve related to layering be observed (see Figure 14c,d). It was concluded that water or other small molecules are necessary for a charging of the mica surface via the dissolution of K<sup>+</sup> ions, inducing a structuring of the ionic liquid at the interface. In additionally wetted ionic liquids, layering was also present, but the jumps between the innermost layer and surface were larger, suggesting that water forms an adsorption layer on the mica surface, altering the interface structure [105].

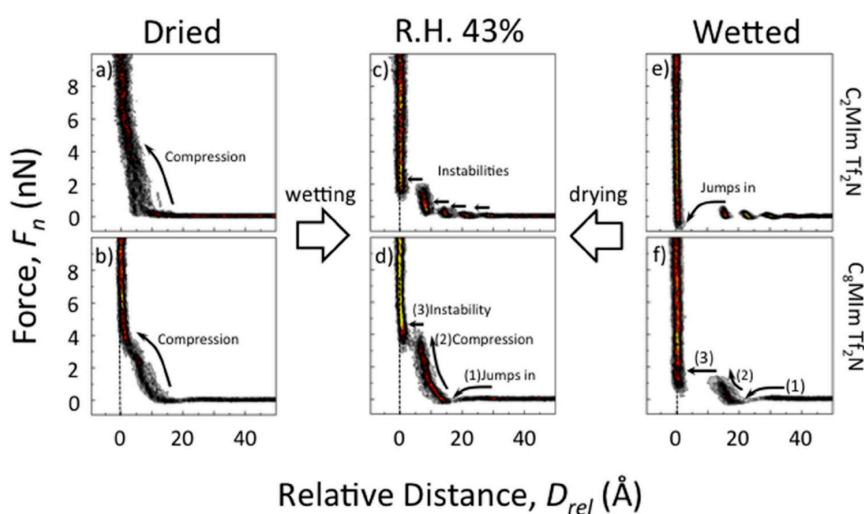


**Figure 14.** Investigation of the interface between mica and [C<sub>2</sub>MIm][TFSI] (a,c,e) and [C<sub>8</sub>Mim][TFSI] (b,d,f) using force-separation histograms at different water contents. Adapted from Cheng et al. [105].

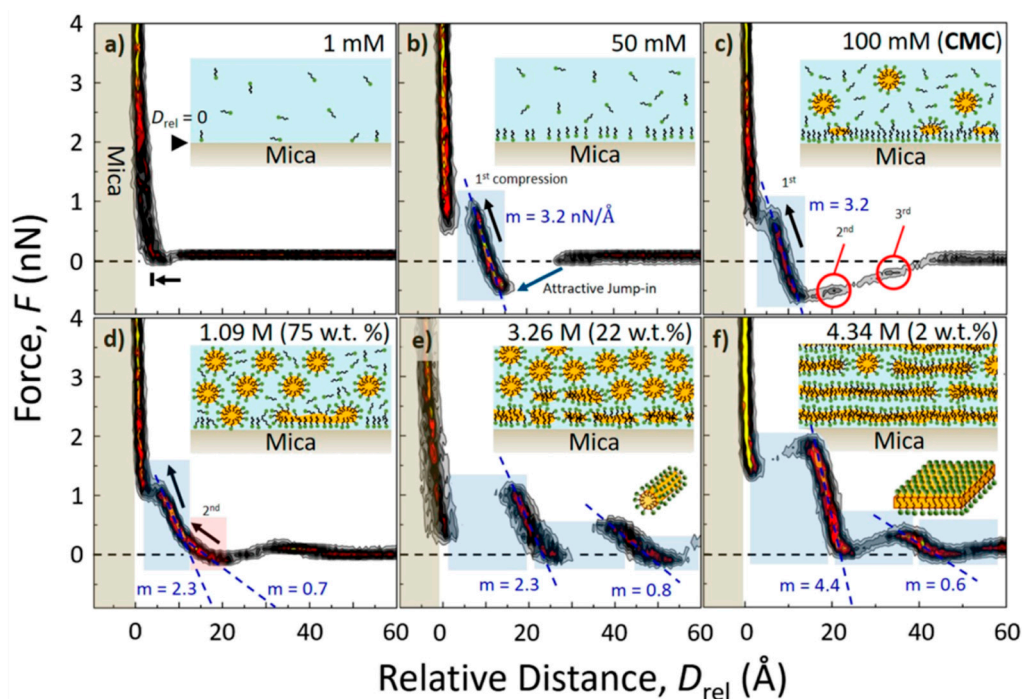


**Figure 15.** AFS investigation of the interface between mica and mixtures of water with different concentrations of  $[C_8MIm][Cl]$ . The force/distance slopes ( $m$ ) corresponding to the stiffness of each layer are shown as blue dotted lines and the schematic structural interpretations are depicted as insets. Adapted with permission from Cheng et al. [113]. Copyright 2018, American Chemical Society.

The effect of higher amounts of water on the interface structure was examined by Cui et al. [114] using 1-ethyl-3-methylimidazolium trifluoromethylsulfonate ( $[EMIm][TfO]$ ) in contact with Au (111). They found that the number of layers detected by the force–separation curves decreased with increasing water content. For the pure ionic liquid, five layers were seen, whereas after the addition of 50 vol% of water, only one layer was resolved under cathodic polarization. Assisted by complementary experiments using vibrational spectroscopy, Cui et al. [114] concluded that a “water in IL” to “IL in water” transition takes place at 20–30 vol%. As a result, the water molecules weakened the interaction between the ions and the multilayer structure at the interface is diluted to a classical Helmholtz-like double layer. Depending on the molecular configuration of the ionic liquids, this transition can also be related to the formation of micelles. Reverting the roles of ionic liquid and water, Cheng et al. [113] investigated the formation of the mica/liquid interface when an ionic liquid, here  $[C_8MIm][Cl]$ , was subsequently added to water. As is shown in Figure 15, force–separation histograms were constructed for different concentrations of the ionic liquid in the mixture. While at a concentration of 1 mM, no dense interface structure was present, the jumps in the force curves setting in at 50 mM indicate the formation of a dense hydrophobic molecular surface layer. At higher concentrations, the amount and position of the jumps was found to be modified, revealing that at first the formation and adsorption of micellar structures occurs and, finally, a dense multilayer interface evolves. This also impacts the compression of the layer calculated as force/distance slopes. At low concentrations of the ionic liquid, a value of 3.2 nN/Å is obtained, which corresponds to a dense surface layer of single molecules. This compression is weakened at an intermediate concentration, indicating a mixture of separated molecules and micelles, while at a high concentration, the compression was found to be the highest at 4.4 nN/Å, reflecting the dense micellar layering.

### 5.3. Addition of Metallic Solvates

As ionic liquids are promising electrolytes for applications containing metallic components such as batteries or electrodeposition, many AFS studies have been performed that focus on the formation of the interface structure in the presence of the dissolved metals. Endres et al. [115] performed a study of [Py<sub>1,4</sub>][FAP] on the Au(111) surface, revealing that the addition of LiCl changes the interface drastically. While the AFM tip experienced a repulsive force when approaching the surface as a pure ionic liquid, an attractive force was present in the Li-containing mixture. The addition of Li only influenced the innermost layer of the interface structure, leaving layers further away from the interface unchanged. Using N-butyl-N-methylpyrrolidinium bis(fluorosulfonyl)imid ([Py<sub>1,4</sub>][FSI]), which intrinsically shows a stronger interaction with the Au(111) surface than [Py<sub>1,4</sub>][FAP], comparable experiments, with the addition of Na, were performed. Carstens et al. [116] reported that the interfacial multilayer structure is not significantly affected after adding small amounts of Na. However, when adding more than 0.25 M of Na, the innermost layers changed, indicating the local formation of [Na(FSI)<sub>3</sub>]<sup>2-</sup>. The impact of a layered electric double layer on the electrochemical performance has also been illustrated by Begić et al. [117], addressing the mechanisms in rechargeable zinc batteries. Zinc dicyanamide salt (Zn(dca)<sub>2</sub>) has been admixed to two ionic liquids, N-butyl-N-methylpyrrolidinium dicyanamide ([C<sub>4</sub>mpyr][dca]) and 1-ethyl-3-methyl-imidazolium dicyanamide ([C<sub>2</sub>mim][dca]), while force–separation curves were recorded as a function of the water content and applied potential. Layering at the interface was readily present in the pure ionic liquids in contact with the HOPG. The admixture of the zinc salts did not lead to a significant dissolution of the multilayer structure; it even increased the number of layers for [C<sub>4</sub>mpyr][dca]. These results demonstrate that interface ordering can be challenging when an effective mass transport to the surface is needed and that for chemically similar ionic liquids, electrochemical performance can significantly differ.

The subtle interplay between metallic precursors and ionic liquids was elucidated by Borisenko et al. [118], looking at the electrodeposition of Ta and Ga from halides in [Py<sub>1,4</sub>][TFSA], as well as [Py<sub>1,4</sub>][FAP] on the Au(111) surface. Using AFS, they concluded that in mixtures of [Py<sub>1,4</sub>][TFSA] and TaF<sub>5</sub>, the electric double layer becomes enriched in Ta-containing molecules, thus allowing for their further reduction to Ta in metallic form directly at the interface. When they tried to reproduce this experiment using [Py<sub>1,4</sub>][FAP], it was not possible to induce the electrodeposition process, as the Ta species was pushed away from the interface. By changing the precursor to GaCl<sub>3</sub>, however, the electrodeposition of Ga could be successfully started in both ionic liquids.

In order to simulate the interaction between solutes and ionic liquids, Hoffmann et al. [119] developed a mathematical semi-continuum model based on AFS investigations of the interface between Au(111) and in [Py<sub>1,4</sub>][TFSA] with varying admixtures of Ag salt. As presented in Figure 16, a clear correlation between Ag concentration and the detected layers at the interface was observable. With increasing Ag concentrations, the widths of the layers at first increase, suggesting the presence of larger AgTFSA complexes within the double layer. Eventually, at concentrations above 500 μM AgTFSA, the ordered structure collapses into a simple double layer. The developed thermodynamic continuum model, which treats the ionic liquid as being composed of hard spheres, could be successfully applied to describe the interfacial structure under the influence of Ag additives and to simulate the force–separation curves [119]. To summarize the investigations of metal additives in different ionic liquids, it can be concluded that, in general, the structured interface layer becomes distorted at high metal concentrations; however, at low and intermediate concentrations, a complex interplay with the metallic species and ionic liquid takes place such that each specific combination of additives and liquids must be considered independently.

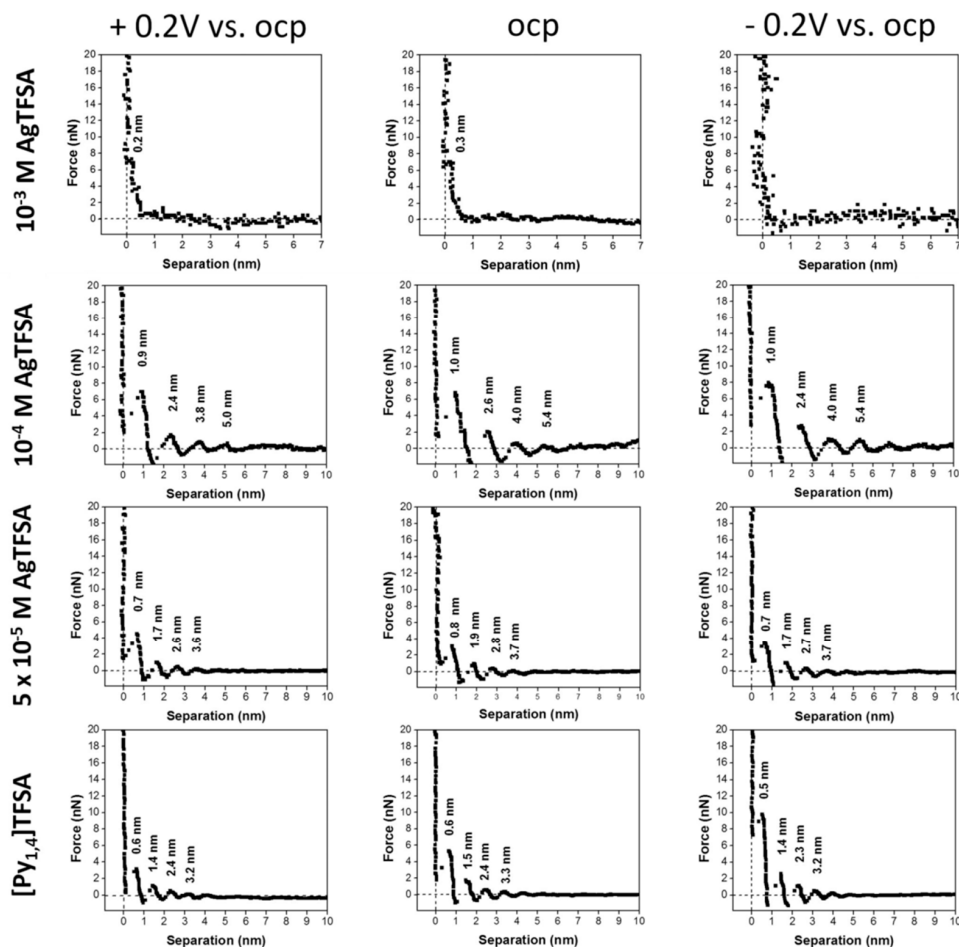


**Figure 16.** Force–separation curves measured in  $[Py_{1,4}][TfSA]$  with different concentrations of Ag on the Au surface. Adapted from Hoffmann et al. [119].

## 6. Towards Three-Dimensional Mapping of the Interface Layer

As the electric double layer not only exhibits a characteristic layered structure in the out-of-plane direction, as illustrated by the AFS examples above, but may also feature in-plane inhomogeneities, three-dimensional mapping is necessary in order to obtain a complete picture of electrochemical interface reactions. Using AFM-based techniques, two approaches to 3D mapping can be distinguished. Either force–separation curves can be recorded at different lateral positions using AFS, or classical AFM scans can be obtained at different separations between tip and surface, thus revealing slices through the liquid. These experiments have been primarily performed using the dynamic AFM modes, employing amplitude modulation (AM) or frequency modulation (FM), which are well-established techniques for mapping surfaces in liquids with atomic resolution [120]. Dynamic AFM has also been successfully applied to monitor the electric double layer in conventional electrolytes [121]. In order to map a solid–liquid interface by AFM, one must ensure a careful sample and tip preparation, an extremely low vibration and noise level, and sufficient thermal stability. Due to these experimental challenges, the number of publications showing 3D data of the interface layer obtained by AFM is small compared to those presenting single point AFS curves.

Using contact-mode AFM, Black et al. [122] performed investigations of defects in the double layer structure between HOPG and  $[EMIm][TfSI]$ , as shown in Figure 17. They measured 20 force–separation curves at positions separated by 25 nm from each other along a defined line across the HOPG surface (see Figure 17a). The resulting curves were compiled into a map providing a cross-section through the interface layer (see Figure 17b). The layered interface structure can be clearly identified here. It can also be seen that distortions of the structure are present in the liquid above the step edges of the HOPG

substrate. In a small region, the ionic layers bend to compensate for the disturbance induced by the topographic defect. This becomes obvious with regard to the force–separation histograms obtained above the basal plane, which show up to five layers (Figure 17c) and above a step edge showing only one layer clearly (Figure 17d). To illustrate the interplay between the topography of the solid surface and the ordering of the ionic liquid, a second region of the HOPG surface was investigated by Black et al. [122], which contained no single step edges but few larger steps, as shown in the topography line scan in Figure 17e. The map of the force–separation curve measured along the line scan shown in Figure 17e reveals the presence of edge dislocations in the ionic liquid interface structure. Those dislocations are present above the basal plane of the substrate and are related to a distortion of the layered structure spreading over 50 nm to 80 nm. This behavior is in correspondence with observations of conventional liquid crystals [123] that also show topological effects, which can have an impact on the electrochemical performance when using ionic liquids.

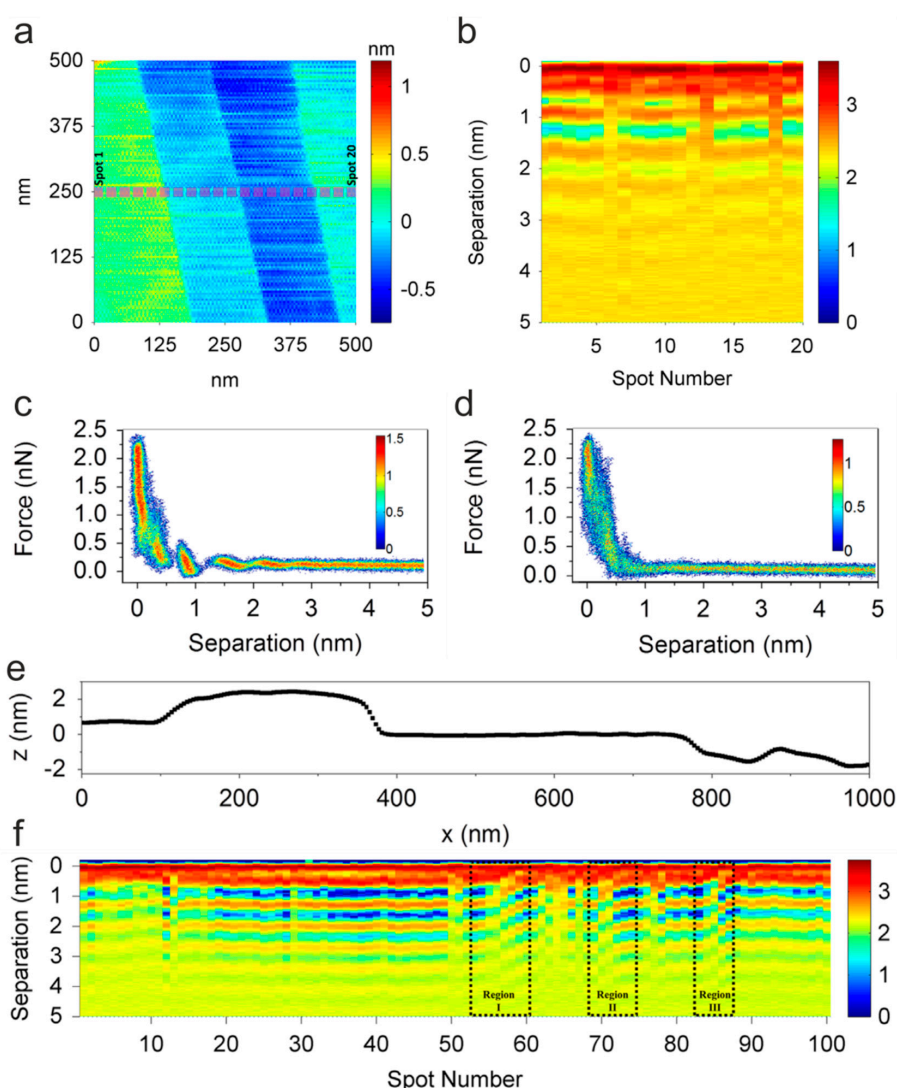


**Figure 17.** Influence of topological defects on the interface structure between highly oriented pyrolytic graphite (HOPG) and [EMIm][TFSI]. (a) Topography of HOPG; (b) force–separation curves measured at 20 points as marked in (a); (c) force–separation histograms obtained on the basal plane; and (d) from the step edge; (e) topography line profile with a length of 1  $\mu\text{m}$ ; (f) force–separation curves measured along the line in (e) showing different defect regions. Adapted with permission from Black et al. [122]. Copyright 2015, Elsevier.

To map the solvation layers in ionic liquids, Negami et al. [124] employed frequency modulation (FM)-AFM force mapping, using a quartz tuning fork as a qPlus sensor, which has a higher  $Q$  factor than standard cantilevers used for the optical lever technique and thus can also provide high resolution in viscous liquids. On the  $[\text{Py}_{1,4}][\text{FAP}]/\text{Au}(111)$  interface, they were able to measure force spectroscopy series by recording frequency shift–separation curves at different positions of the surface. By applying bias to the substrate, they could monitor the changes to the electrical polarization. They found a characteristic ordered solvation structure detected as oscillations in the frequency shift signal, corresponding to the length of an ion pair.

The same FM-AFM technique was applied to the  $[\text{Py}_{1,4}][\text{FAP}]/\text{KCl}(100)$  interface by Ichii et al. [125]. In this study, an alkali-halide substrate was employed, as it forms a neutral surface, having the same quantity of anions and cations in the uppermost surface layer. Hence, a different interface layer structure than that on electrified metal electrodes will form. In Figure 18a, a series of frequency shift–distance curves measured along a line of 4 nm is shown as a 2D map. A distinct oscillation in the frequency shift signal with up to five stripes can be identified. This is illustrated by the cross sections displayed in Figure 18b–e, extracted from the 2D map at four different positions. The distance between the stripes is smaller than the ion pair size of  $[\text{Py}_{1,4}][\text{FAP}]$  and rather corresponds to the lattice constant of KCl. The frequency shift–distance curves exhibit a sawtooth-like pattern with distinct jumps, which is a completely different behavior than that observed by FM-AFM on electrified surfaces and showing sinusoidal curves. Hence, Ichii et al. [125] concluded that those jumps are not related to the existence of solvation layers but are caused by a tip-induced dissolution of the KCl surface in the ionic liquid. This example shows that care must be taken when interpreting force-separation curves and that not all observed step-like features are indicative of the existence of interface layers.

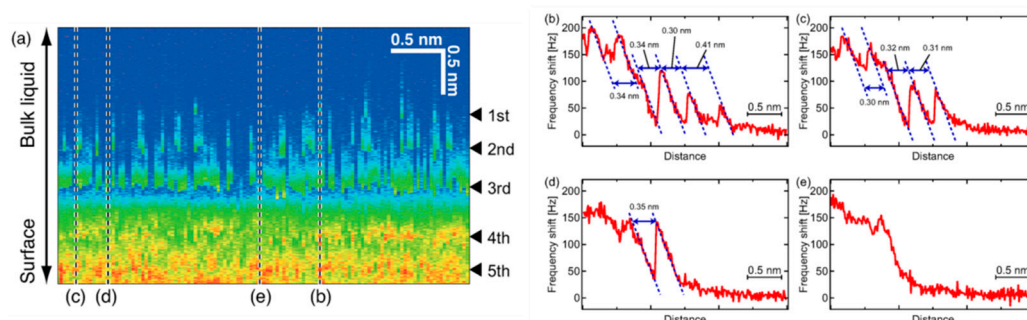


**Figure 18.** Frequency modulation (FM)-AFM investigation of the  $[\text{Py}_{1,4}][\text{FAP}]/\text{KCl}(100)$  interface. (a) Frequency shift–distance curves measured along a distance of 4 nm; (b–e) cross-sections obtained at the lines marked in (a). Adapted with permission from Ichii et al. [125]. Copyright 2014, the American Chemical Society.

A further approach to image the interface structure was followed using AM-AFM. This technique has been successfully applied to image the HOPG/PAN or HOPG/[EMIm][TFSI] interface [126,127]. Two-dimensional maps of the in-plane structure of the interface have been obtained with a high resolution comparable to STM, and a laterally heterogeneous interface layer has been identified. Ebeling et al. [128] extended the AM-AFM investigations on HOPG/PAN to the third dimension by also performing dynamic force spectroscopy. The phase and amplitude were measured as a function of the separation, revealing a layered interface structure. Elbourne et al. [47] applied the combination of AM-AFM mapping and spectroscopy of the five different ionic liquids, ethylammonium nitrate (EAN), propylammonium nitrate (PAN), ethanolanionium nitrate (EtAN), ethylammonium formate (EAF), and  $N,N$ -dimethylethylammonium formate (DMEAF). Phase- and amplitude–separation curves were measured on the mica surface. Complementary AM-AFM maps of the innermost and near-surface layers have been obtained using cantilevers of different stiffness, thus providing spatially-resolved information in three dimensions. The results, shown in Figure 19 provide evidence for a strong influence of molecular configuration of the cation on the interface structure.

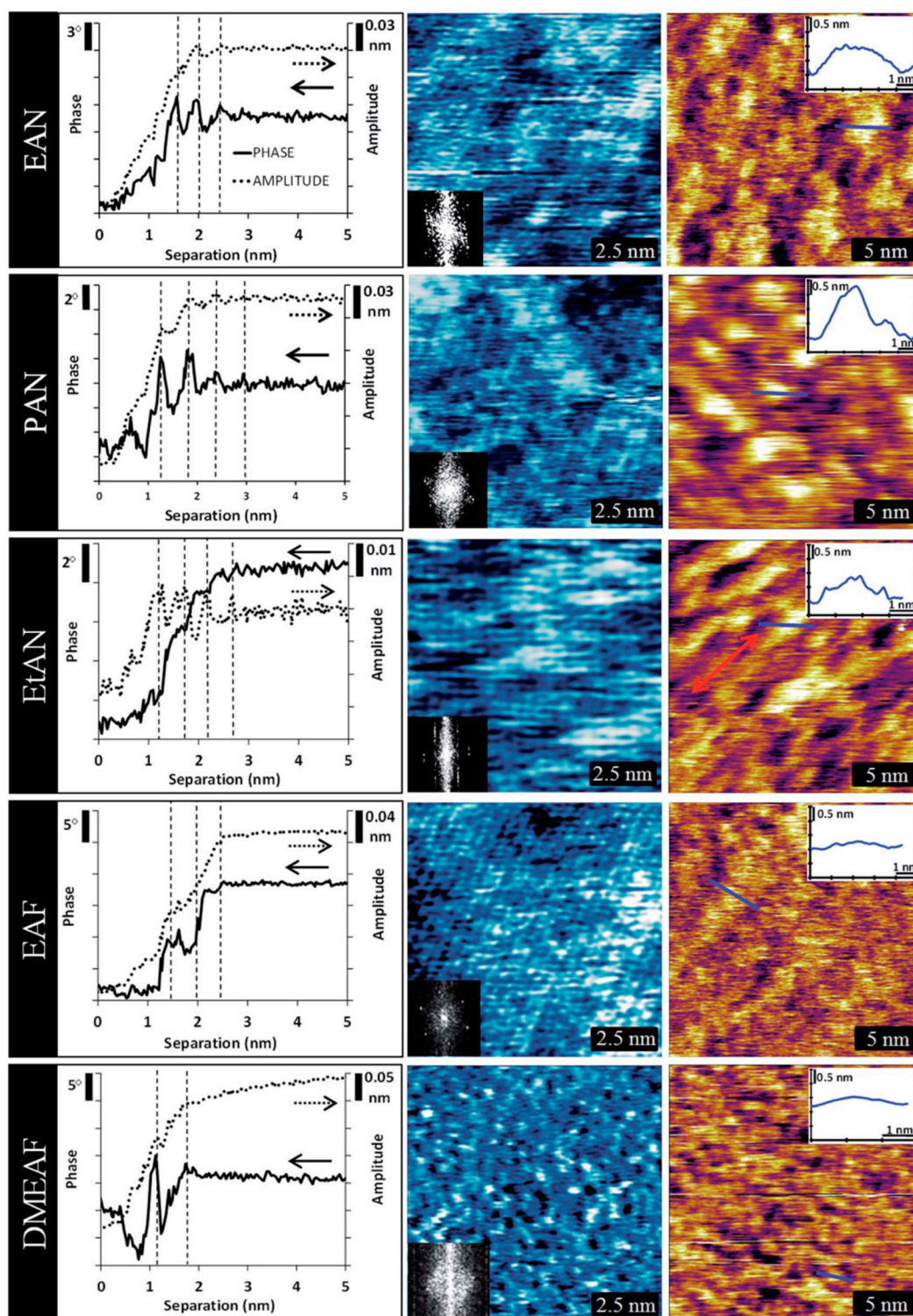


**Figure 19.** Amplitude modulation (AM)-AFM study of the interface between mica and different ionic liquids. Left: Amplitude and phase–separation curves. Right: Topographic images of the innermost (blue) and the first near-surface layer (brown). Adapted from Elbourne et al. [47]—Published by The Royal Society of Chemistry.

It can be seen that cations with short alkyl lengths form a superstructure related to the ionic ordering of the mica surface, providing a template for structuring the innermost layer of the ionic liquid (see center column). For DMEAF, having an additional methyl group in the cation the map of

the innermost layer shows a higher irregularity, indicating that steric effects prevent regular ordering. The near-surface layer shows larger and more disordered features than the innermost layer for all investigated liquids (see right column in Figure 19). The formation of domains with dimensions larger than a single ion pair can be observed as differences in the measured topography. Here, a high topography value corresponds to a high local stiffness of the liquid, while dark areas correspond to regions where the molecules are mobile, such that the damping of the oscillation of the tip-cantilever system is smaller. Comparing the maps obtained in the different ionic liquids, distinct differences in the nanostructure can be identified, confirming that the specific configuration of both the anion and cation determines the morphology of the interface layer.

## 7. Conclusions

Ordered interfacial nanostructures are a common phenomenon between an electrified surface and an ionic liquid. While they were first predicted from indirect experimental evidence and simulations many years ago, the use of atomic force microscopy in spectroscopy mode provides a direct image of the details of the structuring during electrochemical operation. The AFS results available from the literature so far demonstrate that most of the investigated ionic liquids form a layered structure at the interface, thus forming an electric double layer beyond the classical Gouy–Chapman–Stern theory. The specific arrangement at the interface can be quite complex, which relates to the interplay between the Coulomb forces and steric effects caused by the molecular structure of the ions. Impurities and additives, such as water or metallic ions, also have a share in the formation of the nanostructure. At low concentrations of additives, a strengthening of the nanostructure has often been observed, while at higher concentrations, transition to a conventional solute/solvent mixture occurs. However, the details of the interface formation depend significantly on the specific ionic liquid in use, which on the one hand is a challenge when aiming to derive a general picture of the solid/ionic liquid interface, but on the other allows adjustment of the desired interface properties by designing customized ionic liquids.

**Author Contributions:** The manuscript was written through contributions of all authors. All authors have given approval to the final version of the manuscript.

**Funding:** This research received no external funding.

**Acknowledgments:** We gratefully acknowledge C. Wood for proofreading of the manuscript.

**Conflicts of Interest:** The authors declare no conflict of interest.

## References

1. MacFarlane, D.R.; Kar, M.; Pringle, J.M. *Fundamentals of Ionic Liquids: From Chemistry to Applications*; Wiley-VCH: Weinheim, Germany, 2017; ISBN 9783527339990.
2. Welton, T. Room-Temperature Ionic Liquids. Solvents for Synthesis and Catalysis. *Chem. Rev.* **1999**, *99*, 2071–2084. [[CrossRef](#)]
3. Tucker, T.G.; Davidowski, S.K.; Angell, C.A. Inorganic vs Organic Cation Ionic Liquids and Their Solutions with Alkali Metal Containing Ionic Liquids. *J. Electrochem. Soc.* **2017**, *164*, H153–H158. [[CrossRef](#)]
4. Seddon, K.R. Ionic Liquids for Clean Technology. *J. Chem. Technol. Biotechnol.* **1997**, *68*, 351–356. [[CrossRef](#)]
5. Freemantle, M. Designer Solvents. *Chem. Eng. News* **1998**, *76*, 32–37. [[CrossRef](#)]
6. Armand, M.; Endres, F.; MacFarlane, D.R.; Ohno, H.; Scrosati, B. Ionic-liquid materials for the electrochemical challenges of the future. *Nat. Mater.* **2009**, *8*, 621–629. [[CrossRef](#)]
7. Plechkova, N.V.; Seddon, K.R. Applications of ionic liquids in the chemical industry. *Chem. Soc. Rev.* **2008**, *37*, 123–150. [[CrossRef](#)]
8. MacFarlane, D.R.; Tachikawa, N.; Forsyth, M.; Pringle, J.M.; Howlett, P.C.; Elliott, G.D.; Davis, J.H.; Watanabe, M.; Simon, P.; Angell, C.A. Energy applications of ionic liquids. *Energy Environ. Sci.* **2014**, *7*, 232–250. [[CrossRef](#)]
9. Rogers, R.D. Reflections on ionic liquids. *Nature* **2007**, *447*, 917–918. [[CrossRef](#)] [[PubMed](#)]
10. Bernal, J.D. The Bakerian Lecture, 1962 The structure of liquids. *Proc. R. Soc. Lond. Ser. A Math. Phys. Sci.* **1964**, *280*, 299–322.

11. Hayes, R.; Warr, G.G.; Atkin, R. Structure and Nanostructure in Ionic Liquids. *Chem. Rev.* **2015**, *115*, 6357–6426. [[CrossRef](#)]
12. Parsons, R. Models of the Electrical Double Layer. In *Trends in Interfacial Electrochemistry*; Springer: Dordrecht, The Netherlands, 1986; pp. 373–385.
13. Kornyshev, A.A. Double-Layer in Ionic Liquids: Paradigm Change? *J. Phys. Chem. B* **2007**, *111*, 5545–5557. [[CrossRef](#)]
14. Macdonald, D.D. Reflections on the history of electrochemical impedance spectroscopy. *Electrochim. Acta* **2006**, *51*, 1376–1388. [[CrossRef](#)]
15. Baldelli, S. Probing Electric Fields at the Ionic Liquid–Electrode Interface Using Sum Frequency Generation Spectroscopy and Electrochemistry. *J. Phys. Chem. B* **2005**, *109*, 13049–13051. [[CrossRef](#)]
16. Talaty, E.R.; Raja, S.; Storhaug, V.J.; Dölle, A.; Carper, W.R. Raman and Infrared Spectra and ab Initio Calculations of C<sub>2-4</sub>MIM Imidazolium Hexafluorophosphate Ionic Liquids. *J. Phys. Chem. B* **2004**, *108*, 13177–13184. [[CrossRef](#)]
17. Mezger, M.; Schramm, S.; Schröder, H.; Reichert, H.; Deutsch, M.; De Souza, E.J.; Okasinski, J.S.; Ocko, B.M.; Honkimäki, V.; Dosch, H. Layering of [BMIM]<sup>+</sup>-based ionic liquids at a charged sapphire interface. *J. Chem. Phys.* **2009**, *131*, 094701. [[CrossRef](#)]
18. Lauw, Y.; Rodopoulos, T.; Gross, M.; Nelson, A.; Gardner, R.; Horne, M.D. Electrochemical cell for neutron reflectometry studies of the structure of ionic liquids at electrified interface. *Rev. Sci. Instrum.* **2010**, *81*, 074101. [[CrossRef](#)]
19. Liu, Z.; Zhang, P.; Wang, Y.; Kan, Y.; Chen, Y. Surface force apparatus studies on the surface interaction of [C<sub>n</sub>mim<sup>+</sup>][BF<sub>4</sub><sup>-</sup>] and [C<sub>n</sub>mim<sup>+</sup>][PF<sub>6</sub><sup>-</sup>] ionic liquids. In Proceedings of the 2017 IEEE International Conference on Manipulation, Manufacturing and Measurement on the Nanoscale (3M-NANO), Shanghai, China, 7–11 August 2017; pp. 300–304.
20. Black, J.M.; Zhu, M.; Zhang, P.; Unocic, R.R.; Guo, D.; Okatan, M.B.; Dai, S.; Cummings, P.T.; Kalinin, S.V.; Feng, G.; et al. Fundamental aspects of electric double layer force-distance measurements at liquid-solid interfaces using atomic force microscopy. *Sci. Rep.* **2016**, *6*, 32389. [[CrossRef](#)]
21. Canongia Lopes, J.N.A.; Pádua, A.A.H. Nanostructural Organization in Ionic Liquids. *J. Phys. Chem. B* **2006**, *110*, 3330–3335. [[CrossRef](#)]
22. Araque, J.C.; Hettige, J.J.; Margulis, C.J. Modern Room Temperature Ionic Liquids, a Simple Guide to Understanding Their Structure and How It May Relate to Dynamics. *J. Phys. Chem. B* **2015**, *119*, 12727–12740. [[CrossRef](#)] [[PubMed](#)]
23. Dupont, J. On the solid, liquid and solution structural organization of imidazolium ionic liquids. *J. Braz. Chem. Soc.* **2004**, *15*, 341–350. [[CrossRef](#)]
24. Triolo, A.; Russina, O.; Bleif, H.-J.; Di Cola, E. Nanoscale Segregation in Room Temperature Ionic Liquids. *J. Phys. Chem. B* **2007**, *111*, 4641–4644. [[CrossRef](#)] [[PubMed](#)]
25. Dupont, J. From Molten Salts to Ionic Liquids: A “Nano” Journey. *Acc. Chem. Res.* **2011**, *44*, 1223–1231. [[CrossRef](#)]
26. Shimizu, K.; Tariq, M.; Freitas, A.A.; Pádua, A.A.H.; Lopes, J.N.C.; Shimizu, K.; Tariq, M.; Freitas, A.A.; Pádua, A.A.H.; Lopes, J.N.C. Self-Organization in Ionic Liquids: From Bulk to Interfaces and Films. *J. Braz. Chem. Soc.* **2015**, *27*, 349–362. [[CrossRef](#)]
27. Hardacre, C.; Holbrey, J.D.; Nieuwenhuyzen, M.; Youngs, T.G.A. Structure and Solvation in Ionic Liquids. *Acc. Chem. Res.* **2007**, *40*, 1146–1155. [[CrossRef](#)]
28. Wang, Y.; Jiang, W.; Yan, T.; Voth, G.A. Understanding Ionic Liquids through Atomistic and Coarse-Grained Molecular Dynamics Simulations. *Acc. Chem. Res.* **2007**, *40*, 1193–1199. [[CrossRef](#)]
29. Greaves, T.L.; Ha, K.; Muir, B.W.; Howard, S.C.; Weerawardena, A.; Kirby, N.; Drummond, C.J. Protic ionic liquids (PILs) nanostructure and physicochemical properties: Development of high-throughput methodology for PIL creation and property screens. *Phys. Chem. Chem. Phys.* **2015**, *17*, 2357–2365. [[CrossRef](#)]
30. Greaves, T.L.; Drummond, C.J. Protic Ionic Liquids: Evolving Structure–Property Relationships and Expanding Applications. *Chem. Rev.* **2015**, *115*, 11379–11448. [[CrossRef](#)]
31. Henderson, W.A.; Fylstra, P.; De Long, H.C.; Trulove, P.C.; Parsons, S. Crystal structure of the ionic liquid EtNH<sub>3</sub>NO<sub>3</sub>—Insights into the thermal phase behavior of protic ionic liquids. *Phys. Chem. Chem. Phys.* **2012**, *14*, 16041. [[CrossRef](#)]

32. Lo Celso, F.; Appetecchi, G.B.; Jafta, C.J.; Gontrani, L.; Canongia Lopes, J.N.; Triolo, A.; Russina, O. Nanoscale organization in the fluorinated room temperature ionic liquid: Tetraethyl ammonium (trifluoromethanesulfonyl)(nonafluorobutylsulfonyl)imide. *J. Chem. Phys.* **2018**, *148*, 193816. [[CrossRef](#)] [[PubMed](#)]
33. Russina, O.; Lo Celso, F.; Di Michiel, M.; Passerini, S.; Appetecchi, G.B.; Castiglione, F.; Mele, A.; Caminiti, R.; Triolo, A. Mesoscopic structural organization in triphilic room temperature ionic liquids. *Faraday Discuss.* **2013**, *167*, 499. [[CrossRef](#)] [[PubMed](#)]
34. Hettige, J.J.; Araque, J.C.; Margulis, C.J. Bicontinuity and Multiple Length Scale Ordering in Triphilic Hydrogen-Bonding Ionic Liquids. *J. Phys. Chem. B* **2014**, *118*, 12706–12716. [[CrossRef](#)]
35. Seddon, K.R.; Stark, A.; Torres, M.-J. Influence of chloride, water, and organic solvents on the physical properties of ionic liquids. *Pure Appl. Chem.* **2000**, *72*, 2275–2287. [[CrossRef](#)]
36. Chatel, G.; Pereira, J.F.B.; Debbeti, V.; Wang, H.; Rogers, R.D. Mixing ionic liquids—“simple mixtures” or “double salts”? *Green Chem.* **2014**, *16*, 2051. [[CrossRef](#)]
37. Yaghini, N.; Pitawala, J.; Matic, A.; Martinelli, A. Effect of Water on the Local Structure and Phase Behavior of Imidazolium-Based Protic Ionic Liquids. *J. Phys. Chem. B* **2015**, *119*, 1611–1622. [[CrossRef](#)]
38. Niazi, A.A.; Rabideau, B.D.; Ismail, A.E. Effects of Water Concentration on the Structural and Diffusion Properties of Imidazolium-Based Ionic Liquid–Water Mixtures. *J. Phys. Chem. B* **2013**, *117*, 1378–1388. [[CrossRef](#)]
39. Martins, V.L.; Nicolau, B.G.; Urahata, S.M.; Ribeiro, M.C.C.; Torresi, R.M. Influence of the Water Content on the Structure and Physicochemical Properties of an Ionic Liquid and Its Li + Mixture. *J. Phys. Chem. B* **2013**, *117*, 8782–8792. [[CrossRef](#)] [[PubMed](#)]
40. Cao, Y.; Sun, X.; Chen, Y.; Mu, T. Water Sorption in Amino Acid Ionic Liquids: Kinetic, Mechanism, and Correlations between Hygroscopicity and Solvatochromic Parameters. *ACS Sustain. Chem. Eng.* **2014**, *2*, 138–148. [[CrossRef](#)]
41. O’Mahony, A.M.; Silvester, D.S.; Aldous, L.; Hardacre, C.; Compton, R.G. Effect of Water on the Electrochemical Window and Potential Limits of Room-Temperature Ionic Liquids. *J. Chem. Eng. Data* **2008**, *53*, 2884–2891. [[CrossRef](#)]
42. Cao, Y.; Chen, Y.; Sun, X.; Zhang, Z.; Mu, T. Water sorption in ionic liquids: kinetics, mechanisms and hydrophilicity. *Phys. Chem. Chem. Phys.* **2012**, *14*, 12252. [[CrossRef](#)]
43. Chen, Y.; Cao, Y.; Lu, X.; Zhao, C.; Yan, C.; Mu, T. Water sorption in protic ionic liquids: Correlation between hygroscopicity and polarity. *New J. Chem.* **2013**, *37*, 1959. [[CrossRef](#)]
44. Ma, C.; Laaksonen, A.; Liu, C.; Lu, X.; Ji, X. The peculiar effect of water on ionic liquids and deep eutectic solvents. *Chem. Soc. Rev.* **2018**, *47*, 8685–8720. [[CrossRef](#)]
45. Blesic, M.; Marques, M.H.; Plechkova, N.V.; Seddon, K.R.; Rebelo, L.P.N.; Lopes, A. Self-aggregation of ionic liquids: Micelle formation in aqueous solution. *Green Chem.* **2007**, *9*, 481. [[CrossRef](#)]
46. Bica, K.; Gärtner, P.; Gritsch, P.J.; Ressmann, A.K.; Schröder, C.; Zirbs, R. Micellar catalysis in aqueous–ionic liquid systems. *Chem. Commun.* **2012**, *48*, 5013. [[CrossRef](#)]
47. Elbourne, A.; Voitchovsky, K.; Warr, G.G.; Atkin, R. Ion structure controls ionic liquid near-surface and interfacial nanostructure. *Chem. Sci.* **2015**, *6*, 527–536. [[CrossRef](#)]
48. Wippermann, K.; Wackerl, J.; Lehnert, W.; Huber, B.; Korte, C. 2-Sulfoethylammonium Trifluoromethanesulfonate as an Ionic Liquid for High Temperature PEM Fuel Cells. *J. Electrochem. Soc.* **2016**, *163*, F25–F37. [[CrossRef](#)]
49. Helmholtz, H. Ueber einige Gesetze der Vertheilung elektrischer Ströme in körperlichen Leitern mit Anwendung auf die thierisch-elektrischen Versuche. *Ann. der Phys. und Chemie* **1853**, *165*, 211–233. [[CrossRef](#)]
50. Gouy, M. Sur la constitution de la charge électrique à la surface d’un électrolyte. *J. Phys. Théorique Appliquée* **1910**, *9*, 457–468. [[CrossRef](#)]
51. Chapman, D.L. LI. A contribution to the theory of electrocapillarity. *Lond. Edinb. Dublin Philos. Mag. J. Sci.* **1913**, *25*, 475–481. [[CrossRef](#)]
52. Stern, O. Zur Theorie der elektrolytischen Doppelschicht. *Zeitschrift für Elektrochemie und Angew. Phys. Chemie* **1924**, *30*, 508–516.
53. Schmickler, W.; Henderson, D. New models for the structure of the electrochemical interface. *Prog. Surf. Sci.* **1986**, *22*, 323–419. [[CrossRef](#)]

54. Schmickler, W.; Henderson, D. The interphase between jellium and a hard sphere electrolyte. A model for the electric double layer. *J. Chem. Phys.* **1984**, *80*, 3381–3386. [[CrossRef](#)]
55. Badiali, J.P. Contribution of the metal to the differential capacitance of the ideally polarizable electrode. *Electrochim. Acta* **1986**, *31*, 149–154. [[CrossRef](#)]
56. Fedorov, M.V.; Kornyshev, A.A. Ionic Liquids at Electrified Interfaces. *Chem. Rev.* **2014**, *114*, 2978–3036. [[CrossRef](#)]
57. Bazant, M.Z.; Storey, B.D.; Kornyshev, A.A. Double Layer in Ionic Liquids: Overscreening versus Crowding. *Phys. Rev. Lett.* **2011**, *106*, 046102. [[CrossRef](#)]
58. Dong, K.; Liu, X.; Dong, H.; Zhang, X.; Zhang, S. Multiscale Studies on Ionic Liquids. *Chem. Rev.* **2017**, *117*, 6636–6695. [[CrossRef](#)]
59. Merlet, C.; Limmer, D.T.; Salanne, M.; van Roij, R.; Madden, P.A.; Chandler, D.; Rotenberg, B. The Electric Double Layer Has a Life of its Own. *J. Phys. Chem. C* **2014**, *118*, 18291–18298. [[CrossRef](#)]
60. Fedorov, M.V.; Georgi, N.; Kornyshev, A.A. Double layer in ionic liquids: The nature of the camel shape of capacitance. *Electrochem. Commun.* **2010**, *12*, 296–299. [[CrossRef](#)]
61. Gebbie, M.A.; Smith, A.M.; Dobbs, H.A.; Lee, A.A.; Warr, G.G.; Banquy, X.; Valtiner, M.; Rutland, M.W.; Israelachvili, J.N.; Perkin, S.; et al. Long range electrostatic forces in ionic liquids. *Chem. Commun.* **2017**, *53*, 1214–1224. [[CrossRef](#)] [[PubMed](#)]
62. Binnig, G.; Quate, C.F.; Gerber, C. Atomic Force Microscope. *Phys. Rev. Lett.* **1986**, *56*, 930–933. [[CrossRef](#)]
63. Cappella, B.; Dietler, G. Force-distance curves by atomic force microscopy. *Surf. Sci. Rep.* **1999**, *34*, 1–104. [[CrossRef](#)]
64. Schimmel, T.; Koch, T.; Küppers, J.; Lux-Steiner, M. True atomic resolution under ambient conditions obtained by atomic force microscopy in the contact mode. *Appl. Phys. A Mater. Sci. Process.* **1999**, *68*, 399–402. [[CrossRef](#)]
65. Morita, S.; Giessibl, F.J.; Meyer, E.; Wiesendanger, R. (Eds.) *Noncontact Atomic Force Microscopy*; NanoScience and Technology; Springer International Publishing: Cham, The Netherlands, 2015; ISBN 978-3-319-15587-6.
66. Giessibl, F.J. The qPlus sensor, a powerful core for the atomic force microscope. *Rev. Sci. Instrum.* **2019**, *90*, 011101. [[CrossRef](#)]
67. Mungse, H.P.; Ichii, T.; Utsunomiya, T.; Sugimura, H. Investigation of BMI-PF<sub>6</sub> Ionic Liquid/Graphite Interface Using Frequency Modulation Atomic Force Microscopy. *MRS Adv.* **2018**, *3*, 2725–2733. [[CrossRef](#)]
68. Dufrière, Y.F.; Ando, T.; Garcia, R.; Alsteens, D.; Martinez-Martin, D.; Engel, A.; Gerber, C.; Müller, D.J. Imaging modes of atomic force microscopy for application in molecular and cell biology. *Nat. Nanotechnol.* **2017**, *12*, 295–307. [[CrossRef](#)]
69. Liu, Y.; Zhang, Y.; Wu, G.; Hu, J. Coexistence of Liquid and Solid Phases of Bmim-PF<sub>6</sub> Ionic Liquid on Mica Surfaces at Room Temperature. *J. Am. Chem. Soc.* **2006**, *128*, 7456–7457. [[CrossRef](#)] [[PubMed](#)]
70. He, P.; Liu, H.; Li, Z.; Li, J. Electrodeposition of Platinum in Room-Temperature Ionic Liquids and Electrocatalytic Effect on Electro-oxidation of Methanol. *J. Electrochem. Soc.* **2005**, *152*, E146. [[CrossRef](#)]
71. Atkin, R.; Warr, G.G. Self-Assembly of a Nonionic Surfactant at the Graphite/Ionic Liquid Interface. *J. Am. Chem. Soc.* **2005**, *127*, 11940–11941. [[CrossRef](#)]
72. Kubo, K.; Hirai, N.; Tanaka, T.; Hara, S. Decay of nano-islands located on Au(1 0 0) electrode in room temperature molten salt (EMImBF<sub>4</sub>). *Surf. Sci.* **2004**, *565*, L271–L276. [[CrossRef](#)]
73. Kubo, K.; Hirai, N.; Tanaka, T.; Hara, S. In situ observation on Au(1 0 0) surface in molten EMImBF<sub>4</sub> by electrochemical atomic force microscopy (EC-AFM). *Surf. Sci.* **2003**, *546*, L785–L788. [[CrossRef](#)]
74. Seo, Y.; Jhe, W. Atomic force microscopy and spectroscopy. *Rep. Prog. Phys.* **2008**, *71*, 016101. [[CrossRef](#)]
75. Takeyasu, K. (Ed.) *Atomic Force Microscopy in Nanobiology*; Jenny Stanford Publishing: Singapore, 2016; ISBN 9780429074219.
76. Trewby, W.; Livesey, D.; Voitchovsky, K. Buffering agents modify the hydration landscape at charged interfaces. *Soft Matter* **2016**, *12*, 2642–2651. [[CrossRef](#)]
77. Senden, T.J. Force microscopy and surface interactions. *Curr. Opin. Colloid Interface Sci.* **2001**, *6*, 95–101. [[CrossRef](#)]
78. Burnham, N.A.; Colton, R.J.; Pollock, H.M. Interpretation of force curves in force microscopy. *Nanotechnology* **1993**, *4*, 64–80. [[CrossRef](#)]

79. Leite, F.L.; Bueno, C.C.; Da Róz, A.L.; Ziemath, E.C.; Oliveira, O.N.; Leite, F.L.; Bueno, C.C.; Da Róz, A.L.; Ziemath, E.C.; Oliveira, O.N. Theoretical Models for Surface Forces and Adhesion and Their Measurement Using Atomic Force Microscopy. *Int. J. Mol. Sci.* **2012**, *13*, 12773–12856. [[CrossRef](#)] [[PubMed](#)]
80. Perkin, S. Ionic liquids in confined geometries. *Phys. Chem. Chem. Phys.* **2012**, *14*, 5052. [[CrossRef](#)]
81. Amano, K.; Yokota, Y.; Ichii, T.; Yoshida, N.; Nishi, N.; Katakura, S.; Imanishi, A.; Fukui, K.; Sakka, T. A relationship between the force curve measured by atomic force microscopy in an ionic liquid and its density distribution on a substrate. *Phys. Chem. Chem. Phys.* **2017**, *19*, 30504–30512. [[CrossRef](#)]
82. Akrami, S.M.R.; Nakayachi, H.; Watanabe-Nakayama, T.; Asakawa, H.; Fukuma, T. Significant improvements in stability and reproducibility of atomic-scale atomic force microscopy in liquid. *Nanotechnology* **2014**, *25*, 455701. [[CrossRef](#)]
83. Lo, Y.-S.; Huefner, N.D.; Chan, W.S.; Dryden, P.; Hagenhoff, B.; Beebe, T.P. Organic and Inorganic Contamination on Commercial AFM Cantilevers. *Langmuir* **1999**, *15*, 6522–6526. [[CrossRef](#)]
84. Gołek, F.; Mazur, P.; Ryszka, Z.; Zuber, S. AFM image artifacts. *Appl. Surf. Sci.* **2014**, *304*, 11–19. [[CrossRef](#)]
85. Zhong, Y.-X.; Yan, J.-W.; Li, M.-G.; Zhang, X.; He, D.-W.; Mao, B.-W. Resolving Fine Structures of the Electric Double Layer of Electrochemical Interfaces in Ionic Liquids with an AFM Tip Modification Strategy. *J. Am. Chem. Soc.* **2014**, *136*, 14682–14685. [[CrossRef](#)]
86. Best, R.B.; Brockwell, D.J.; Toca-Herrera, J.L.; Blake, A.W.; Smith, D.A.; Radford, S.E.; Clarke, J. Force mode atomic force microscopy as a tool for protein folding studies. *Anal. Chim. Acta* **2003**, *479*, 87–105. [[CrossRef](#)]
87. Brockwell, D.J.; Paci, E.; Zinober, R.C.; Beddard, G.S.; Olmsted, P.D.; Smith, D.A.; Perham, R.N.; Radford, S.E. Pulling geometry defines the mechanical resistance of a  $\beta$ -sheet protein. *Nat. Struct. Mol. Biol.* **2003**, *10*, 731–737. [[CrossRef](#)]
88. Atkin, R.; Warr, G.G. Structure in Confined Room-Temperature Ionic Liquids. *J. Phys. Chem. C* **2007**, *111*, 5162–5168. [[CrossRef](#)]
89. Hayes, R.; Borisenko, N.; Tam, M.K.; Howlett, P.C.; Endres, F.; Atkin, R. Double Layer Structure of Ionic Liquids at the Au(111) Electrode Interface: An Atomic Force Microscopy Investigation. *J. Phys. Chem. C* **2011**, *115*, 6855–6863. [[CrossRef](#)]
90. Hoth, J.; Hausen, F.; Müser, M.H.; Bennewitz, R. Force microscopy of layering and friction in an ionic liquid. *J. Phys. Condens. Matter* **2014**, *26*, 284110. [[CrossRef](#)]
91. Hayes, R.; Warr, G.G.; Atkin, R. At the interface: Solvation and designing ionic liquids. *Phys. Chem. Chem. Phys.* **2010**, *12*, 1709. [[CrossRef](#)]
92. Yan, J.-W.; Tian, Z.-Q.; Mao, B.-W. Molecular-level understanding of electric double layer in ionic liquids. *Curr. Opin. Electrochem.* **2017**, *4*, 105–111. [[CrossRef](#)]
93. Zhang, X.; Zhong, Y.-X.; Yan, J.-W.; Su, Y.-Z.; Zhang, M.; Mao, B.-W. Probing double layer structures of Au (111)–BMIPF<sub>6</sub> ionic liquid interfaces from potential-dependent AFM force curves. *Chem. Commun.* **2012**, *48*, 582–584. [[CrossRef](#)] [[PubMed](#)]
94. Atkin, R.; Borisenko, N.; Drüschler, M.; Endres, F.; Hayes, R.; Huber, B.; Roling, B. Structure and dynamics of the interfacial layer between ionic liquids and electrode materials. *J. Mol. Liq.* **2014**, *192*, 44–54. [[CrossRef](#)]
95. Atkin, R.; Borisenko, N.; Drüschler, M.; El Abedin, S.Z.; Endres, F.; Hayes, R.; Huber, B.; Roling, B. An in situ STM/AFM and impedance spectroscopy study of the extremely pure 1-butyl-1-methylpyrrolidinium tris(pentafluoroethyl)trifluorophosphate/Au(111) interface: Potential dependent solvation layers and the herringbone reconstruction. *Phys. Chem. Chem. Phys.* **2011**, *13*, 6849. [[CrossRef](#)]
96. Atkin, R.; El Abedin, S.Z.; Hayes, R.; Gasparotto, L.H.S.; Borisenko, N.; Endres, F. AFM and STM Studies on the Surface Interaction of [BMP]TfSA and [EMIm]TfSA Ionic Liquids with Au(111). *J. Phys. Chem. C* **2009**, *113*, 13266–13272. [[CrossRef](#)]
97. Liu, Z.; Cui, T.; Lu, T.; Shapouri Ghazvini, M.; Endres, F. Anion Effects on the Solid/Ionic Liquid Interface and the Electrodeposition of Zinc. *J. Phys. Chem. C* **2016**, *120*, 20224–20231. [[CrossRef](#)]
98. Werzer, O.; Warr, G.G.; Atkin, R. Compact Poly(ethylene oxide) Structures Adsorbed at the Ethylammonium Nitrate–Silica Interface. *Langmuir* **2011**, *27*, 3541–3549. [[CrossRef](#)]
99. Li, H.; Endres, F.; Atkin, R. Effect of alkyl chain length and anion species on the interfacial nanostructure of ionic liquids at the Au(111)–ionic liquid interface as a function of potential. *Phys. Chem. Chem. Phys.* **2013**, *15*, 14624. [[CrossRef](#)]
100. Lewandowski, A.; Olejniczak, A.; Galinski, M.; Stepniak, I. Performance of carbon–carbon supercapacitors based on organic, aqueous and ionic liquid electrolytes. *J. Power Sources* **2010**, *195*, 5814–5819. [[CrossRef](#)]

101. Black, J.M.; Walters, D.; Labuda, A.; Feng, G.; Hillesheim, P.C.; Dai, S.; Cummings, P.T.; Kalinin, S.V.; Proksch, R.; Balke, N. Bias-Dependent Molecular-Level Structure of Electrical Double Layer in Ionic Liquid on Graphite. *Nano Lett.* **2013**, *13*, 5954–5960. [[CrossRef](#)]
102. Jurado, L.A.; Espinosa-Marzal, R.M. Insight into the Electrical Double Layer of an Ionic Liquid on Graphene. *Sci. Rep.* **2017**, *7*, 4225. [[CrossRef](#)] [[PubMed](#)]
103. Sheehan, A.; Jurado, L.A.; Ramakrishna, S.N.; Arcifa, A.; Rossi, A.; Spencer, N.D.; Espinosa-Marzal, R.M. Layering of ionic liquids on rough surfaces. *Nanoscale* **2016**, *8*, 4094–4106. [[CrossRef](#)]
104. Radiom, M.; Pedraz, P.; Pilkington, G.; Rohlmann, P.; Glavatskih, S.; Rutland, M.; Radiom, M.; Pedraz, P.; Pilkington, G.; Rohlmann, P.; et al. Anomalous Interfacial Structuring of a Non-Halogenated Ionic Liquid: Effect of Substrate and Temperature. *Colloids Interfaces* **2018**, *2*, 60. [[CrossRef](#)]
105. Cheng, H.-W.; Dienemann, J.-N.; Stock, P.; Merola, C.; Chen, Y.-J.; Valtiner, M. The Effect of Water and Confinement on Self-Assembly of Imidazolium Based Ionic Liquids at Mica Interfaces. *Sci. Rep.* **2016**, *6*, 30058. [[CrossRef](#)] [[PubMed](#)]
106. Jurado, L.A.; Kim, H.; Rossi, A.; Arcifa, A.; Schuh, J.K.; Spencer, N.D.; Leal, C.; Ewoldt, R.H.; Espinosa-Marzal, R.M. Effect of the environmental humidity on the bulk, interfacial and nanoconfined properties of an ionic liquid. *Phys. Chem. Chem. Phys.* **2016**, *18*, 22719–22730. [[CrossRef](#)]
107. Broderick, A.; Newberg, J.T. Water at Ionic Liquid Interfaces. In *Ionic Liquids: Current State and Future Directions*; Shiflett, M.B., Scurto, A.M., Eds.; ACS Publications: Washington, DC, USA, 2017; pp. 227–249.
108. Bi, S.; Wang, R.; Liu, S.; Yan, J.; Mao, B.; Kornyshev, A.A.; Feng, G. Minimizing the electrosorption of water from humid ionic liquids on electrodes. *Nat. Commun.* **2018**, *9*, 5222. [[CrossRef](#)]
109. Zhong, Y.; Yan, J.; Li, M.; Chen, L.; Mao, B. The Electric Double Layer in an Ionic Liquid Incorporated with Water Molecules: Atomic Force Microscopy Force Curve Study. *ChemElectroChem* **2016**, *3*, 2221–2226. [[CrossRef](#)]
110. Wang, Z.; Li, H.; Atkin, R.; Priest, C. Influence of Water on the Interfacial Nanostructure and Wetting of [Rmim][NTf<sub>2</sub>] Ionic Liquids at Mica Surfaces. *Langmuir* **2016**, *32*, 8818–8825. [[CrossRef](#)]
111. Wang, Z.; Shi, F.; Zhao, C. Humidity-accelerated spreading of ionic liquids on a mica surface. *RSC Adv.* **2017**, *7*, 42718–42724. [[CrossRef](#)]
112. Kawada, S.; Kodama, E.; Sato, K.; Ogawa, S.; Watanabe, M.; Okubo, H.; Sasaki, S. Effect of water on the interfacial structures of room-temperature ionic liquids. *Surf. Interface Anal.* **2019**, *51*, 17–20. [[CrossRef](#)]
113. Cheng, H.-W.; Weiss, H.; Stock, P.; Chen, Y.-J.; Reinecke, C.R.; Dienemann, J.-N.; Mezger, M.; Valtiner, M. Effect of Concentration on the Interfacial and Bulk Structure of Ionic Liquids in Aqueous Solution. *Langmuir* **2018**, *34*, 2637–2646. [[CrossRef](#)] [[PubMed](#)]
114. Cui, T.; Lahiri, A.; Carstens, T.; Borisenko, N.; Pulletikurthi, G.; Kuhl, C.; Endres, F. Influence of Water on the Electrified Ionic Liquid/Solid Interface: A Direct Observation of the Transition from a Multilayered Structure to a Double-Layer Structure. *J. Phys. Chem. C* **2016**, *120*, 9341–9349. [[CrossRef](#)]
115. Endres, F.; Borisenko, N.; El Abedin, S.Z.; Hayes, R.; Atkin, R. The interface ionic liquid(s)/electrode(s): In situ STM and AFM measurements. *Faraday Discuss.* **2012**, *154*, 221–233. [[CrossRef](#)]
116. Carstens, T.; Lahiri, A.; Borisenko, N.; Endres, F. [Py<sub>1,4</sub>]FSI-NaFSI-Based Ionic Liquid Electrolyte for Sodium Batteries: Na<sup>+</sup> Solvation and Interfacial Nanostructure on Au(111). *J. Phys. Chem. C* **2016**, *120*, 14736–14741. [[CrossRef](#)]
117. Begić, S.; Li, H.; Atkin, R.; Hollenkamp, A.F.; Howlett, P.C. A comparative AFM study of the interfacial nanostructure in imidazolium or pyrrolidinium ionic liquid electrolytes for zinc electrochemical systems. *Phys. Chem. Chem. Phys.* **2016**, *18*, 29337–29347. [[CrossRef](#)]
118. Borisenko, N.; Lahiri, A.; Pulletikurthi, G.; Cui, T.; Carstens, T.; Zahlbach, J.; Atkin, R.; Endres, F. The Au(111)/IL interfacial nanostructure in the presence of precursors and its influence on the electrodeposition process. *Faraday Discuss.* **2018**, *206*, 459–473. [[CrossRef](#)]
119. Hoffmann, V.; Pulletikurthi, G.; Carstens, T.; Lahiri, A.; Borodin, A.; Schammer, M.; Horstmann, B.; Latz, A.; Endres, F. Influence of a silver salt on the nanostructure of a Au(111)/ionic liquid interface: An atomic force microscopy study and theoretical concepts. *Phys. Chem. Chem. Phys.* **2018**, *20*, 4760–4771. [[CrossRef](#)]
120. Fukuma, T.; Kobayashi, K.; Matsushige, K.; Yamada, H. True atomic resolution in liquid by frequency-modulation atomic force microscopy. *Appl. Phys. Lett.* **2005**, *87*, 034101. [[CrossRef](#)]

121. Siretanu, I.; Ebeling, D.; Andersson, M.P.; Stipp, S.L.S.; Philipse, A.; Stuart, M.C.; van den Ende, D.; Mugele, F. Direct observation of ionic structure at solid-liquid interfaces: A deep look into the Stern Layer. *Sci. Rep.* **2015**, *4*, 4956. [[CrossRef](#)] [[PubMed](#)]
122. Black, J.M.; Baris Okatan, M.; Feng, G.; Cummings, P.T.; Kalinin, S.V.; Balke, N. Topological defects in electric double layers of ionic liquids at carbon interfaces. *Nano Energy* **2015**, *15*, 737–745. [[CrossRef](#)]
123. Jain, S. Shilpa Defects and Order in Liquid Crystal Phases. Ph.D. Thesis, Harvard University, Cambridge, MA, USA, 1999.
124. Negami, M.; Ichii, T.; Murase, K.; Sugimura, H. Visualization of Ionic-Liquid/Solid Interfaces by Frequency Modulation Atomic Force Microscopy. *ECS Trans.* **2013**, *50*, 349–355. [[CrossRef](#)]
125. Ichii, T.; Negami, M.; Sugimura, H. Atomic-Resolution Imaging on Alkali Halide Surfaces in Viscous Ionic Liquid Using Frequency Modulation Atomic Force Microscopy. *J. Phys. Chem. C* **2014**, *118*, 26803–26807. [[CrossRef](#)]
126. Page, A.J.; Elbourne, A.; Stefanovic, R.; Addicoat, M.A.; Warr, G.G.; Voitchovsky, K.; Atkin, R. 3-Dimensional atomic scale structure of the ionic liquid–graphite interface elucidated by AM-AFM and quantum chemical simulations. *Nanoscale* **2014**, *6*, 8100–8106. [[CrossRef](#)]
127. Elbourne, A.; McDonald, S.; Voichovsky, K.; Endres, F.; Warr, G.G.; Atkin, R. Nanostructure of the Ionic Liquid–Graphite Stern Layer. *ACS Nano* **2015**, *9*, 7608–7620. [[CrossRef](#)]
128. Ebeling, D.; Bradler, S.; Roling, B.; Schirmeisen, A. 3-Dimensional Structure of a Prototypical Ionic Liquid–Solid Interface: Ionic Crystal-Like Behavior Induced by Molecule–Substrate Interactions. *J. Phys. Chem. C* **2016**, *120*, 11947–11955. [[CrossRef](#)]



© 2019 by the authors. Licensee MDPI, Basel, Switzerland. This article is an open access article distributed under the terms and conditions of the Creative Commons Attribution (CC BY) license (<http://creativecommons.org/licenses/by/4.0/>).